# DISTRIBUTED ALGORITHMS FOR VOLTAGE CONTROL IN ELECTRICAL NETWORKS

BY

BRETT A. ROBBINS

THESIS

Submitted in partial fulfillment of the requirements
for the degree of Master of Science in Electrical and Computer Engineering
in the Graduate College of the
University of Illinois at Urbana-Champaign, 2011

Urbana, Illinois

Adviser:

Assistant Professor Alejandro D. Domínguez-García

# ABSTRACT

This thesis proposes a method to utilize distributed energy resources to provide the reactive power support required to stabilize and control voltage in electric power systems. As the number of distributed energy resources continues to increase, traditional approaches to the design and control of distribution networks will no longer be adequate. For example, on a clear day with high incident irradiance, it is possible for the active power injections from photovoltaic systems to reverse the flow of power and cause over-voltages on certain buses. The impacts of photovoltaic systems and plug-in hybrid electric vehicles on distribution networks are of particular interest due to the potentially high penetration of these devices in the years to come. Although the contribution of each device is small, collectively, they can have a significant impact on system reliability and performance. Since the placement and number of these devices are unknown to system operators, a decentralized-distributed control strategy is desired to determine the reactive power support provided for ancillary services. This thesis presents a resource allocation algorithm and an adpative algorithm that modifies its behavior to respond to voltage limits on a radial line. The ability of these distributed algorithms to control voltages is illustrated in a series of case studies.

*To my wife and parents*

# ACKNOWLEDGMENTS

I would like to give special thanks to my adviser, Assistant Professor Alejandro Domínguez-García. His patience and guidance has made this work possible. I would also like to thank Professor Sauer for all of the advice he has given me through my undergraduate and graduate academic careers.

Finally, I would like to thank my family and friends for their continued support. Mom and Dad, thank you for providing me the encouragement and resources that have enabled me to pursue my dreams. Even when I decided to indulge my automotive interests, you kept me on a path that led me to where I am today. My loving wife, thank you for allowing me to pursue my passions and dealing with a husband who is constantly traveling or away. I promise I'll make it up to you.

# CONTENTS

# LIST OF TABLES

# LIST OF FIGURES

# Chapter 1

# INTRODUCTION

Distribution systems, in particular, are subject to several emerging technologies that have the potential to provide ancillary services to the grid that they are connected to [1–5]. For example, plug-in hybrid electric vehicles (PHEV) and other energy storage devices can be used to provide active power for up and down regulation for energy peak-shaving during the day and load-leveling at night [3,6–8]. Although the primary purpose of distributed energy resources (DERs) is to produce active power, they can also be utilized to provide reactive power support. In a power system, the flow of reactive power directly impacts the bus voltages and is critical for voltage stability and control [9,10]. Thus, through the proper coordination and control of their power electronics grid interfaces, these devices could provide the necessary reactive power support to control certain bus voltages and keep the system operating within specifications, i.e., operational requirements constrain bus voltages within $\pm 5\%$ of their nominal values.

Wind technologies and photovoltaic (PV) systems are two of the fastest growing renewable energy markets. According to the 2009 market report published by the National Renewable Energy Laboratory (NREL), the United States installed a capacity of 8.558 GW of wind turbines with $16 billion invested in 2008. This put the cumulative generation capacity for the country at 25.369 GW and effectively made the U.S. the world leader in wind generation [11]. PV installations are experiencing record growth, as well, with a compound annual growth rate of 46% for the past decade (1998-2008). In 2008, an unexpectedly large capacity of 6 GW of PV was installed internationally, compared to the 2.7 GW that was installed in 2007. At this time the U.S. had an installed capacity of 1.1 GW for PV systems where 0.79 GW was grid connected [12]. These trends of record investments in renewable energy sources are expected to continue. The U.S. is projected to have an installed capacity of PV in the range of 6.5 GW by 2015. Similarly, it is forecast that

50% of the houses in Japan will have PV installed according to the PV2030 roadmap [13].

Renewable energy sources inherently introduce uncertainty into the electrical grid. Historically, distribution systems have been overdesigned [14] and the penetration of renewables has been small enough that their control is rather limited. As a result, current regulations require DERs to be controlled so as to maintain a constant power factor, follow scheduled dispatches from an operator, and disconnect from the grid when a fault occurs [15]. With the introduction of DERs, particularly PV, distribution systems will be increasingly pushed to their limits. On a clear day, a high penetration of PV installations has the potential to cause voltage rise and a reversal of active power flow, where the distribution system has a net generation instead of load [13, 16, 17]. Similarly, PV generation of active power can ramp up on the order of 15% of its capacity per minute across the distribution system on days with intermittent sunlight exposure. Limit violations are traditionally handled by tap-changing under load (TCUL) transformers, set voltage regulators (SVR), and fixed/switch capacitors that are either controlled by timers or manually through the Supervisory Control and Data Acquisition (SCADA) systems [18, 19]. However, using the existing equipment to handle the constant variability of the DERs would dramatically reduce the lifetime of these components, which leaves a solution that utilizes the inverters to be desired [16].

## 1.1 Background and Related Work

Proposed solutions to the control DERs include having a centralized strategy, where DERs communicate directly to a central controller, or a hierarchical approach that allows the central controller to communicate indirectly with each DER through other devices. The work in [20] proposes a hierarchical method where the system is grouped into members, referred to as reactive support groups, that belong to a chain of command structure much like the Incident Command System (ICS) used by emergency personal. Each DER is indirectly controlled by a centralized controller that prioritizes dispatch commands relative to the sensitivities of the system.

The authors in [2] propose a multiagent scheme that provides reactive

power support in distribution feeders, and assumes that DERs have two-way communications with a central controller either directly or through other DERs. Agents are assigned to be managers or contractors that bid on reactive power contributions determined by the bus sensitivities. [21] partitions the system buses in groups, or agents, and develops several algorithms that solve the local optimal power flow.

The work in [4] proposes an alternative strategy for controlling DERs. Rather than a centralized controller communicating with every device on the network, a leader node can send requests to a few of these devices, or nodes, that are part of a mesh network. Through an iterative process, DERs determine their power injections so that their collective contributions have the same effect as a centralized control strategy. The coordination controller can be part of a hierarchical or centralized strategy to interact with other areas, but local variables, i.e., bus voltage, can be maintained in a decentralized manner independently from the rest of the network. This control strategy offers many potential benefits over a centralized strategy: (i) it is more economical because it does not require a significant communication infrastructure overlay, (ii) the system is more resilient to faults or unpredictable node behavior, (iii) local information is sufficient to control the devices, and (iv) as new DERs are connected to the network, they can adopt a "plug and play" strategy for syncing with existing devices. The work in this thesis implements these results and illustrates them in a case study. Additionally, these concepts are advanced through an adaptive algorithm and nodes that self-initialize so that a leader node is no longer necessary.

This problem has many similarities with consensus algorithms that have been studied extensively in the field of control (e.g., see [22] and the references therein). The purpose of consensus algorithms is for the agents in a network to agree upon the value of a desired variable given a specific set of initial conditions, e.g., a group of sensors measuring the temperature of a room. The coordination algorithms proposed in this paper differ in two key ways: (i) the nodes are working towards a common goal and each node has its own set of constraints, i.e., capacity limits, so the contribution of the nodes will vary across the network, and (ii) the resulting transition matrices describing the dynamics of the proposed coordination algorithms are column stochastic; thus, the node sums remain constant at each step of the algorithm, whereas with consensus algorithms, the node sums do not remain constant unless the

algorithm solves the average-consensus problem [22].

## 1.2 Chapter Summary and Thesis Organization

This chapter introduced proposed techniques for DERs to provide reactive power support control bus voltages. The intention of this thesis is to develop a decentralized voltage control methodology that will allow devices to be added or removed, while operating in an environment that does not require global knowledge of the system. The remainder of this thesis is organized as follows:

Chapter 2 presents the concepts required for modeling large distribution systems and the mathematical foundation necessary for the distributed algorithms. The irregular nature of distributions systems with their unbalanced loads and poor convergence properties require a different approach to computing power flow. Additionally, a brief review is presented on graph theory and its relationships with convergence properties of nonnegative matrices to define the general form of the distributed algorithms. The material on the analysis of distribution networks can be found in [14]. The general information on power systems throughout this thesis is from [9, 10, 23]. The material on graph theory and nonnegative matrices can be found in [24–27].

In Chapter 3, the fair splitting algorithm from [4] is generalized for all nonnegative matrices that satisfy the properties discussed in Chapter 2. The fair splitting algorithm manages constrained resource allocations, so a localized control strategy is developed and is demonstrated in a 6 bus case study.

Chapter 4 formulates the distributed algorithm for voltage control in a decentralized environment. The methodology uses an adaptive, parametrized transition matrix that updates its value based on current voltage measurements. This allows resource contributions to reach a steady-state solution that satisfies the voltage profile of radial networks.

In Chapter 5, the distributed algorithm is implemented in a series of case studies. The load profiles used for the 8 bus and 123 bus distribution networks are modeled to include a high penetration of photovoltaic systems as well as the additional loads introduced by plug-in hybrid electric vehicles. The distribution systems are modified so that they are operating near their voltage limits, and the ability of the DERs to provide reactive power support to

correct for limit violations is observed.

The final chapter summarizes the contributions of this work. Finally, topics for future research related to this work are discussed.

# Chapter 2

# MODELING FRAMEWORK

## 2.1 Introduction

The following chapter is split into two parts. The first discusses a methodology tailored for large radial, unbalanced distribution systems. Given certain simplifications, conventional power flow methods are sufficient, but are inadequate once this work is extended to three-phase unbalanced networks. The second part reviews the mathematical tools required from graph theory and nonnegative matrices for the distributed algorithms presented in subsequent chapters.

## 2.2 The Ladder Iterative Technique

Traditionally, power flow is computed with the Newton-Rhapson method, or simplified techniques that still require a matrix inverse [10]. Unlike transmission systems, buses in distribution systems are not interconnected with one another and have a radial topology consisting of a large number of sublaterals that are single, two, or three-phase. As a result, distribution networks are inherently unbalanced, and common power flow and analysis techniques are no longer adequate due to poor convergence characteristics [14, 21].

The ladder iterative technique is an algorithm developed specifically to compute power flow for radial networks. This method relies heavily on Kirchhoff's current law (KCL) and Kirchhoff's voltage law (KVL) to perform a series of forward and backward sweeps to converge to a solution. Figure 2.1 is a generalized four node, nonlinear ladder network that will be used to demonstrate how to compute power flow.

At any given bus $m$, the load can either be linear, in the form $z_m = r + jx$

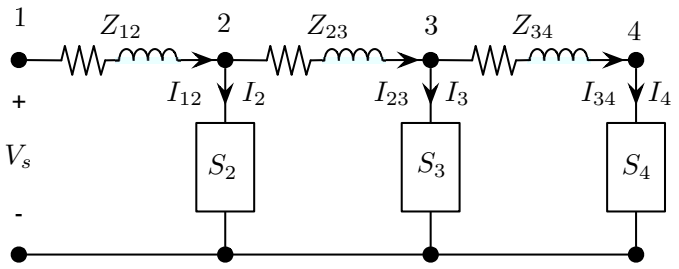


Figure 2.1: Four Node Nonlinear Example

with voltage $V_m$ , or nonlinear with a complex power $S_m = P_m + jQ_m$. The established sign convention will be a load is $S_m < 0$ and the rated power for a source is $S_m > 0$. Let $V_s$ be the voltage of the feeder for the radial line. The ladder iterative technique begins with a forward sweep from the node furthest from the feeder. Initially, it is assumed that $V_4 = V_s$. The current at node 4 is

$$I_4 = \left(\frac{S_4}{V_4}\right)^*. \tag{2.1}$$

By KCL $I_{34} = I_4$. KVL is used to determine the voltage at bus 3 by

$$V_3 = I_{34} * Z_{34} + V_4. \tag{2.2}$$

Similarly, $I_3$ is computed as in (2.1). Therefore, the current from bus 2 to bus 3 is $I_{23} = I_3 + I_{34}$ by KCL. KVL is used to compute $V_2$ with (2.2). This process is repeated to compute $V_1$. The forward sweep uses KVL and KCL to compute the line currents in the network from the initial conditions used for the nodes furthest from feeder.

Once $V_1$ is computed, its value is compared to its specified value $V_s$. If the error is within the desired tolerance, the algorithm is complete. Otherwise, the backward sweep begins. The backward sweep determines bus voltages from the line currents computed in the forward sweep. First, $V_1$ is set to $V_s$ and $V_2$ is computed by

$$V_2 = V_1 - I_{12} * Z_{12}. \tag{2.3}$$

This process repeats until the last bus voltage is computed. Next, the forward sweep initializes using $V_4$ computed from the backward sweep. The ladder iterative technique continues to perform forward and backward sweeps until the solution converges within a specified tolerance. Note that the algorithm

always ends on a forward sweep.

## 2.3 Power Flow

For an unbalanced three-phase network, the topology and the procedure for the algorithm will remain the same. However, the voltages and complex powers will be represented by $3 \times 1$ matrices. The line impedance and currents will be $3 \times 3$ matrices. The mutual impedance terms of the impedance must be considered since the transmission lines in a distributions system are untransposed. The three-phase models for the transmission lines are presented in [14, 21]. Note that the line currents in single and two phase sublaterals associated with the missing phases are set to zero. For the remainder of this thesis, the distribution systems presented are assumed to be single phase.

Figure 2.2 shows a generalized distribution network. Node 1 is the feeder and assumed to be the reference voltage $V_s$ for the network. For the power flow computations, the nodes at the end of the sublaterals are identified, which are buses {6, 9, 11, 13}, and their voltages are set to $V_s$. Nodes {4, 5, 7, 10} are defined as junction nodes since the laterals branch into multiple directions at these points.

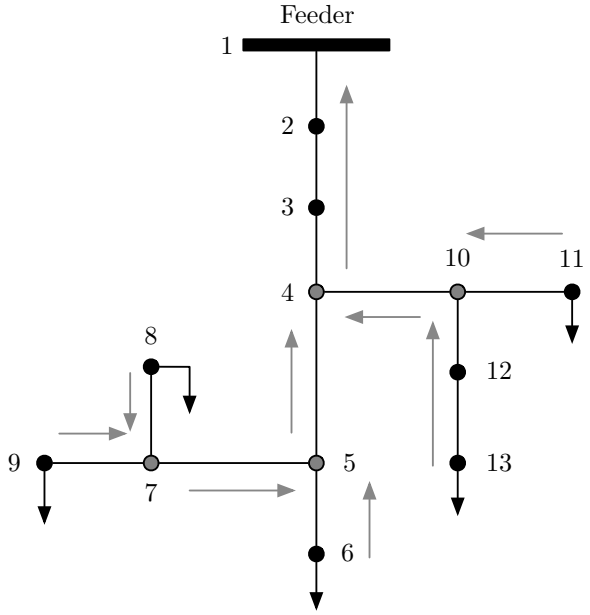


Figure 2.2: Distribution Network

The forward sweep begins by sequentially solving for the line currents from the nodes at the end of the sublaterals until a junction node is reached. For example, the line currents from node 13 to node 10 are solved, followed by the line current from node 11 to node 10. This continues until the first level of junction nodes is reached. At this point, the new end points and junction nodes are determined. Figure 2.3 shows the modified network once the initial line currents are solved.

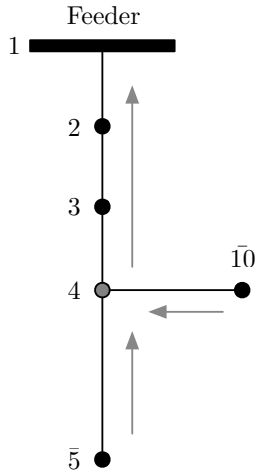


Figure 2.3: Modified Distribution Network

This procedure will repeat until all of the line currents are determined. If the $V_1$ is within a specified tolerance of $V_s$, the algorithm is done. If not, the backward sweep begins by setting $V_1 = V_s$. The bus voltages are computed from the line currents with (2.2) and follow the reversal of the order used in the forward sweep. The combination forward and backwards sweep will continue until the bus voltages converge.

## 2.4 Graph Theoretic Notions

The network describing the feasible exchange of information between nodes can be represented by a graph $\mathcal{G} = \{\mathcal{V}, \mathcal{E}\}$, with $\mathcal{V} = \{1, 2, ..., n\}$ the set of vertices for each node, and $\mathcal{E} \subseteq \mathcal{V} \times \mathcal{V}$ the set of directed edges, where $(j, i) \in \mathcal{E}$ is the order pairs of nodes such that node $j$ receives information from node $i$. Edges can either be directed (also known as arcs), i.e., $(j, i) \in \mathcal{E}$ does not imply that $(i, j) \in \mathcal{E}$; or they can be undirected, i.e., if $(j, i) \in \mathcal{E}$,

then $(i, j) \in \mathcal{E}$. All nodes that can send information to node $j$ are said to be neighbors of node $j$. The set of neighbors of $j$, denoted by $\mathcal{N}_j$, is given by

$$\mathcal{N}_j := \{i \in \mathcal{V} \, : \, (j, i) \in \mathcal{E}\} \, . \tag{2.4}$$

In a graph $\mathcal{G}$, the number of nodes that have $j$ as a neighbor, or where $j$ is the head of an arc, is the in-degree $D_j^-$ of $j$. On the other hand, the number of nodes that $j$ transmits to, or where $j$ is the tail of an arc, is the out-degree $D_j^+$ of $j$. Let $\mathcal{X} \subset \mathcal{V}$ , then $\mathcal{G}$ is considered to be strongly connected if $D_{\mathcal{X}}^- \neq 0$ and $D_{\mathcal{X}}^+ \neq 0$ for every nonempty $\mathcal{X}$ that is a proper subset of $\mathcal{V}$. In other words, a graph is strongly connected if there exists a path from node $i$ to node $j$ $\forall i$, $j = 1, 2, \ldots, n$ [25]. Furthermore, the directed path from node $i$ to $j$ is of finite length for all $i$, $j \in \mathcal{V}$ [24]. Figure 2.4 is an example of a strongly connected graph. There is an undirected edge between nodes 1 and 2, and directed edges are $(3, 2)$ and $(1, 3)$. Nodes 1 and 3 also have self-loops, which will play an important role for the convergence of nonnegative matrices.

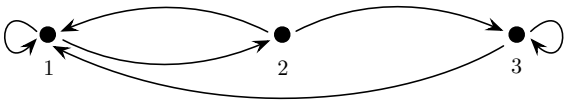


Figure 2.4: 3 Node Graph

## 2.5 The General Form of the Distributed Algorithms and Nonnegative Matrices

Let $\mu_j[k]$, $k = 0, 1, 2, \ldots$ be a quantity of interest that node $j$ needs to compute to fulfill a desired request. In order to update its value from $\mu_j[k]$ to $\mu_j[k+1]$, node $j$ performs linear iterations of the form

$$\mu_j \left[k+1\right] \;\; = \;\; p_{jj}\mu_j \left[k\right] + \sum_{i \in N_j} p_{ji}\mu_i \left[k\right], \tag{2.5}$$

where $p_{ii}$ represents the portion of its value that node $j$ keeps from time-step $k$, and $p_{ji}$ represents the portion of its value that node $i$ transmits to

node $j$ from time-step $k$. The $p_{ji}$'s are assigned such that $\sum_{i=1}^{n} p_{ji}[k] = 1$ $\forall j = 1 \ldots n$. This linear set of equations can be rewritten in the form

$$\mu[k+1] = P_c \mu[k], \tag{2.6}$$

where $P_c \in \mathbb{R}^{n \times n}$ is a column stochastic matrix and $\mu[k] \in \mathbb{R}^n$ is a column vector.

The structure of this setup closely resembles that of a Markov chain. Therefore, analysis tools for Markov chains can be used to develop distributed control algorithms and analyze their convergence properties. In a Markov chain, the state transition matrix must be primitive to ensure that all initial distributions converge to an invariant distribution. To accomplish this, the graph $\mathcal{G}$ associated with the network is required to be strongly connected and have at least one node $i$ with a self-loop where $p_{ii} > 0$. A strongly connected graph is equivalent to a single, irreducible communicating class. The self-loop ensures that at least one node, or state, is aperiodic, which implies that every node in the graph is aperiodic [26]. Also, the Perron-Frobenius theorem[1] for nonnegative matrices ensures that $P_c$ has a unique eigenvalue of maximum modulus at $\lambda_1 = 1$, and that $|\lambda_i| < 1$ $\forall i = 2, 3, \ldots, n$ [24]. Therefore, $\mu[k]$ will always converge asymptotically to the unique solution

$$\lim_{k \to \infty} \mu^{ss}[k] = \left( \sum_{i=1}^{n} \mu_i[0] \right) \pi, \tag{2.7}$$

where $\mu[0]$ is the initial measure (elements do not necessary sum to one) and $\pi \in \mathbb{R}^n$ is the invariant distribution that satisfies $\pi = P_c \pi$, which will be used later in the design of the algorithm. A key idea in the distributed control algorithm we propose is that $P_c$ must be column stochastic so that $\sum_{i=1}^{n} \mu_i[k]$ remains constant $\forall k \geq 0$.

## 2.6 Chapter Summary

In this chapter, the methodology required to compute three-phase unbalanced, radial power systems with poor convergence characteristics was presented. Next, fundamental properties from graph theory and nonnegative

[1] Refer to Appendix A for further definitions

matrices are used to develop the generalized version of the distributed algorithms. The topics presented in this chapter are considered the background knowledge for the algorithms and case studies presented.

# Chapter 3

# LOCALIZED VOLTAGE CONTROL

## 3.1 Introduction

This chapter extends the work from [4]. The control architecture for a localized controller at the distribution feeder is developed. The fair splitting algorithm for resource allocation generalized for any convergent nonnegative matrix is presented. These concepts are illustrated through a case study of a 6 bus transmission network.

## 3.2 Control Architecture

Figure 3.1 illustrates the proposed architecture of the power system, the coordination controller, and the mesh network describing the exchange of information among DERs connected to a system bus. The power system is comprised of a total of $n$ electrical buses, with $m$ generator buses and $(n-m)$ load buses, on the left and right sides of the Network block, respectively. This particular architecture uses bus voltage to determine the amount of reactive power that must be provided by the DERs. On load bus $i$, voltage $V_i$ is measured, compared to reference voltage $V_i^{ref}$, and the error passed to the coordination controller (see Section 3.3 for details), which computes $\rho_d$—the reactive power demand. A request command is sent to the leader node(s) to determine the initial measure $\mu[0] = \rho_d \mu_0$ for the distributed control algorithm. Suppose that the leader node can communicate with $l$ nodes, then the initial distribution is defined as $\mu_0 = [1/l, \ldots, 1/l, 0, \ldots, 0]'$. Each node runs the distributed algorithm that converges asymptotically to the desired solution. The column stochasticity condition enforced in (2.6) ensures that the sum of $\mu_j[k]$ remains constant and equal to $\rho_d$, $\forall k \geq 0$. The

power injections of the DERs sum to $P_i^d + jQ_i^d$, and the perceived load by the rest of the network for computing power flow is $(P_i + P_i^d) + j(Q_i + Q_i^d)$. Assuming that the DERs can meet the coordination controller request $\rho_d$, $Q_i^d$ is explicitly defined. In the context of this paper, the active power $P_i^d$ provided by the DERs is not controlled. However, similarly to reactive power support for voltage control, active power can potentially be used to provide up and down regulation services for frequency control.

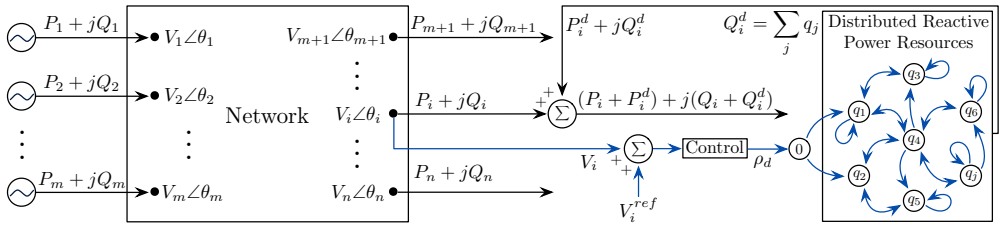


Figure 3.1: System Architecture for the Proposed Distributed Control

## 3.3 Coordination Controller

Figure 3.2 is the block diagram of the feedback control for the coordination controller design. The plant models the dynamics of the DERs from Fig. 3.1. The sensor on the feedback loop is equivalent to the voltage on bus $i$ due to operating conditions in the power system, and thus $V_i$ can be obtained through the power flow equations. For the purpose of designing the coordination controller, the following assumptions are made: (i) the dynamics of the plant are significantly faster than the controller, so the plant is modeled as a constant, $G_{plant} = 1$, (ii) the difference between phase angles of bus $i$ and bus $k$ is very small $\forall i, k = 1, \ldots, n$, and (iii) the voltage sensitivities with respect to changes in the operating point do not change much for different operating points, so the nominal values are used to design the controller. Since the dynamics of the machines were not modeled, a proportional-integral controller is sufficient to control this system.

In an $n$ bus power system, the complex power at bus $i$ is computed by

$$S(x)_i = P_i(x) + jQ_i(x) = V_i \sum_{k \in N_k} V_k e^{j(\theta_i - \theta_k)} Y_{ik}^*, \tag{3.1}$$

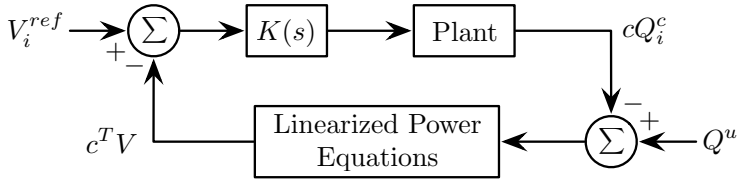


Figure 3.2: Block Diagram for the Coordination Controller Design

where $N_k := \{j \,|\, i \text{ and } j \text{ are directly connected}\}$, $x = [\theta^T \; V^T]^T$ are the independent variables, and the transmission line admittance $Y$ has the form $G + jB$ [10]. The linearized Taylor series expansion of the power equations around an operating point $x^*$ is

$$\begin{aligned} S(x) &= S(x^*) + \nabla S(x^*)(x - x^*) + h.o.t. \\ &\approx S(x^*) + \nabla S(x^*)(x - x^*). \end{aligned} \tag{3.2}$$

Let $V \in \mathbb{R}^n$ be the vector of voltage magnitudes for the $n$ buses. It was assumed that $\theta_i \approx \theta_k$, which implies (3.2) is not dependent on $\theta$, so $x = V$. Therefore, for some constant $\gamma \in \mathbb{R}^n$,

$$V = imag\left(\nabla^{-1} S(x^*)\right) Q + \gamma. \tag{3.3}$$

Let $c \in \mathbb{R}^n$ be a column vector of all zeros except for $c_i = 1$.

The discrete-time controller is obtained from the bilinear transformation

$$H_T(z) = H(s)\big|_{s=\frac{2}{T}\frac{z-1}{z+1}}, \tag{3.4}$$

where $T$ is the sample period [28]. Let $Q_i^c$ be the controllable reactive power injected by the DERs on bus $i$ and $Q^u \in \mathbb{R}^n$ be the uncontrollable reactive power consumed or supplied on the buses. Since the DERs reduce the amount of reactive power consumed on load bus $i$, $c \times Q_i^c$ is subtracted from $Q^u$ and the gains, $K_p$ and $K_i$, are positive. The voltage on bus $i$ is

$$\begin{aligned} V_i(s) &= c^T imag\left(\nabla^{-1} S(x^*)\right) \times \\ &\quad \left[Q^u - cK(s)\left(V_i^{ref} - V_i\right)\right] + c^T \gamma. \end{aligned} \tag{3.5}$$

Define the constants $\alpha := -c^T imag(\nabla^{-1} S(x^*))c > 0$ and

$\beta := c^T imag(\nabla^{-1} S(x^*))Q^u + c^T\gamma$. Then (3.5) simplifies to

$$V_i(s) = \frac{\alpha K(s)}{1+\alpha K(s)} V_i^{ref} + \frac{\beta}{1+\alpha K(s)}. \tag{3.6}$$

The controller transfer function is $K(s) := K_p + K_i/s$. As long as the pole(s) for the system are stable, $\beta$ will decay exponentially to zero. The pole of the system is $s = -\alpha K_i/(1+\alpha K_p)$. For the input-output transfer function, the zero is at $s = -K_i/K_p$. To ensure that the system is stable and settles quickly, $K_i$ and $K_p$ are chosen such that $K_i \gg K_p > 0$. The sample period $T$ needs to be selected such that the distributed algorithm has sufficient time to converge. For example, if each step of the distributed algorithm requires $t$ seconds and no more than $N$ steps to converge within a tolerance $\pm\epsilon$, then an appropriate choice for the sample period is $T > Nt$.

## 3.4 Fair Splitting Algorithm

The proposed distributed control algorithm takes advantage of the graph-theoretic and Markov chain notions introduced in. The state transition matrix for the mesh network topology is designed so that it is column stochastic and primitive—these are sufficient conditions to ensure that the algorithm will converge and the system has a single eigenvalue at $\lambda_1 = 1$.

Each node $j$ will update its value from $\mu_j[k]$ to $\mu_j[k+1]$ as follows

$$\mu_j[k+1] = \frac{1}{1+D_j^+}\mu_j[k] + \sum_{i\in N_j} \frac{1}{1+D_i^+}\mu_i[k], \tag{3.7}$$

where $D_j^+$ is the out-degree of node $j$. The choice of the weights in (3.7) ensures that $P_c$ is column stochastic.

### 3.4.1 Unconstrained Case

Let $\mu_0 \in \mathbb{R}^n$ be the initial distribution, e.g., $\mu_0 = [1/l, \ldots, 1/l, 0, \ldots, 0]'$. For the case where there are not constraints on the maximum capacity that the nodes can provide, the initial measure for demand $\rho_d$ is $\mu[0] = \rho_d\mu_0$, and the system will asymptotically converge to $\mu^{ss} = \rho_d\pi$.

### 3.4.2 Constrained Case

Suppose that each node $i$ has a limit for the amount of reactive power that they can produce, which is denoted by $\mu_i^{max}$. Define $\mu^{max} \in \mathbb{R}^n$ as the vector of the maximum capacities for the $n$ nodes. The reactive power support capacity of the DERs is $\chi = \sum_{i=1}^{n} \mu_i^{max}$. In the constrained case, there may exist some $i$ such that $\rho_d \pi_i > \mu_i^{max}$, so the solution $\mu^{ss} = \rho_d \pi$ may no longer be valid. Assume that $\rho_d < \chi$, then a feasible solution is

$$\mu^{ss} = \frac{\rho_d}{\chi} \mu^{max}. \tag{3.8}$$

The ratio of the demanded reactive power to the network capacity determines the percentage of each resource's capacity that is required by the coordination controller. Since the nodes have access to only local information, $\rho_d/\chi$ has to be obtained iteratively by each node. If $\hat{\mu}[0] = \rho_d \mu_0$, then the system converges to $\hat{\mu}^{ss} = \rho_d \pi$. Similarly, if $\bar{\mu}[0] = \mu^{max}$, then the steady-state solution is $\bar{\mu}^{ss} = \chi \pi$. These solutions can be obtained by computing (2.6) twice in parallel with the appropriate choice of initial measures. Therefore the distributed control algorithm that each node uses to compute the solution for the constrained case is

$$\mu_i[k] \;=\; \frac{\hat{\mu}_i[k]}{\bar{\mu}_i[k]} \mu_i^{max}, \tag{3.9}$$

which converges asymptotically:

$$\lim_{k \to \infty} \mu[k] = \frac{\rho_d}{\chi} \mu^{max}. \tag{3.10}$$

Note that $\bar{\mu}_i[k] > 0$ and $\hat{\mu}_i[k] \geq 0 \; \forall i, k$ because $P_c$ is column stochastic and nonnegative. The algorithm (3.9) is a new result and generalizes algorithm 1 from [4] to directed graphs.

If $\rho_d \leq \chi$, then this solution is guaranteed to adhere to node capacities and is computed iteratively without global knowledge of the mesh network. The strength of this algorithm is its simplicity. As long as the second largest eigenvalue of $P_c$ is small, the algorithm can compute a solution that accounts for node capacity quickly and without any modifications to the state transition matrix. If $\rho_d > \chi$, then the calculated $\mu_i^{ss}$ by each node will be larger than its capacity, so each node $i$ will fix its contribution to be $\mu_i^{ss} = \mu_i^{max}$.

## 3.5 Case Study

A case study was performed with the Western System Coordinating Council (WSCC) standard 3 machine, 9 bus power system model [23]. The model was simplified to 6 buses by removing the transformers. Figure 3.3 describes the topology for the simplified WSCC system.

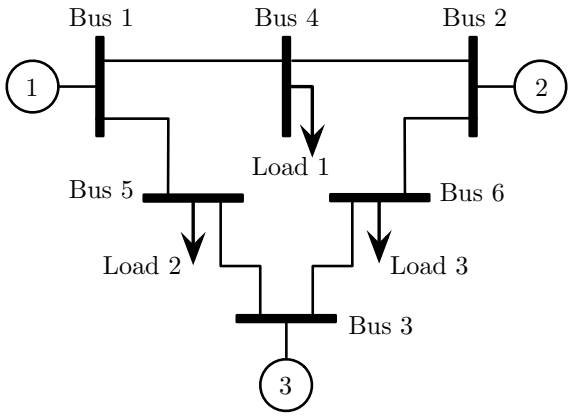


Figure 3.3: Simplified WSCC 3 Machine, 6 Bus System

It was assumed that the system is lossless by setting the transmission line resistance to zero. Table 3.1 lists the values for the transmission lines. The values for the nominal power flow calculation prior to a contingency are listed in Table 3.2, where bus 1 is the system slack bus. Under ideal conditions, generator 3 on bus 3 is operating at its full capacity.

Table 3.1: Transmission Line Values

| From | To | $R$ | $X$ |
|---|---|---|---|
| 1 | 4 | 0 | 0.0720 |
| 2 | 4 | 0 | 0.1008 |
| 1 | 5 | 0 | 0.1610 |
| 2 | 6 | 0 | 0.1700 |
| 3 | 5 | 0 | 0.0850 |
| 3 | 6 | 0 | 0.0920 |

At time $t = 5$ s, generator 2 is disconnected from the system and is switched from a PV bus to a PQ bus with zero load. For the system to be considered

Table 3.2: WSCC System Nominal Power Flow Values

| Bus | $V$ | $\theta$ | $P_g$ | $Q_g$ | $P_l$ | $Q_l$ |
|---|---|---|---|---|---|---|
| 1 | 1 | 0 | 1.5840 | 0.5388 | 0 | 0 |
| 2 | 1 | -1.6406 | 0.8500 | 0.3458 | 0 | 0 |
| 3 | 0.9916 | -5.9563 | 0.7160 | 0.5500 | 0 | 0 |
| 4 | 0.9841 | -3.1300 | 0 | 0 | 1.00 | 0.35 |
| 5 | 0.9617 | -8.0622 | 0 | 0 | 1.25 | 0.50 |
| 6 | 0.9740 | -7.6144 | 0 | 0 | 0.90 | 0.30 |

within acceptable operating conditions, the bus voltages are required to be within $\pm 5\%$ the nominal voltage of 1 p.u., otherwise, a system failure is observed.

Two control architectures were used to test the ability of the DERs to provide reactive power support to stabilize and recover the bus voltages:

a. Only bus 6 was able to provide reactive power support through the coordination of the DERs.

b. All of the load buses are able to provide reactive power through the coordination of the DERs.

Additionally, the simulation was run with and without node capacity constraints on the amount of reactive power the DERs would inject.

### 3.5.1 Distributed Control Algorithm

For simplicity, the four-node network in Fig. 3.4 was used for the network topology of the DERs on any given load bus. The number of DERs attached to each bus is irrelevant, and the convergence time of the distributed control algorithm will not be hampered, e.g., a properly defined network of 10,000 nodes will not affect the simulation results.

The algorithm begins when the leader node splits the demand from the coordination controller to nodes 1 and 2, so the initial measure is $\mu[0] = \rho_d \times [0.5,\ 0.5,\ 0,\ 0]'$, where $\rho_d$ is the demand from the coordination controller. Following (3.7), the state transition matrix that describes the algorithm is given by

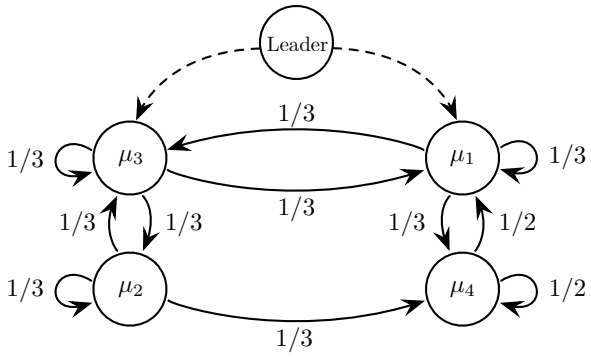


Figure 3.4: Four-Node Network Topology

$$P_c = \begin{bmatrix} 1/3 & 1/3 & 1/3 & 0 \\ 1/3 & 1/3 & 0 & 1/2 \\ 1/3 & 0 & 1/3 & 0 \\ 0 & 1/3 & 1/3 & 1/2 \end{bmatrix}. \tag{3.11}$$

The maximum capacities for the nodes in the constrained case are $\mu^{max} = [0.04,\ 0.02,\ 0.04,\ 0.01]'$, and the network capacity is $\chi = 0.11$. The invariant distribution of $P_c$ is $\pi = [0.231,\ 0.346,\ 0.115,\ 0.308]'$ . The solution to the non-adaptive fair splitting algorithm is $\mu^{ss} = \rho_d \times [0.364,\ 0.182,\ 0.364,\ 0.091]'$ while $\rho_d \leq 0.11$. Otherwise, the solution is $\mu^{ss} = \mu^{max}$ for $\rho_d > 0.11$.

### 3.5.2 Coordination Controller

The time for each iterative step of the distributed control algorithm was set to 10 ms. Let the initial distribution be $\mu[0] = [0.5,\ 0.5,\ 0,\ 0]'$ and $\epsilon = 0.001$. Then for $\mu[k+1] = P_c\mu[k]$, $\mu_i[k] \in (\mu_i^{ss} - \epsilon,\ \mu_i^{ss} + \epsilon)\ \forall i$ after 10 simulation steps, so the sample period of the discrete coordination controller has a lower limit of 1 ms. The sample period $T = 1$ s was selected and guarantees the solution converges within $\pm\epsilon$ of the limit.

For the simplified WSCC system, the value $\alpha$ from (3.6) varies between 0.065 and 0.2. The gains were assigned to be $K_i = 5.5\ \text{s}^{-1}$ and $K_p = 1$ and achieve settling times that are approximately 10 s.

### 3.5.3 Simulation Results

#### 3.5.3.1 Base Case: No Reactive Power Control

Figure 3.5 shows the bus voltages from the base case. Generator 3 was already operating at its maximum capacity prior to the contingency, so it switches to a PQ bus at time $t = 5$ s. Therefore, generator 1 is required to produce the difference in real and reactive power caused due to the loss of generator 2. The contingency causes a voltage drop on every bus except for the slack bus. Based on the topology of the system, bus 6 is the load bus most sensitive to failures on bus 2 and bus 3, and experiences the most significant voltage drop after the contingency. The system is considered failed with bus 5 and bus 6 outside specifications at 0.9421 p.u. and 0.9399 p.u., respectively.

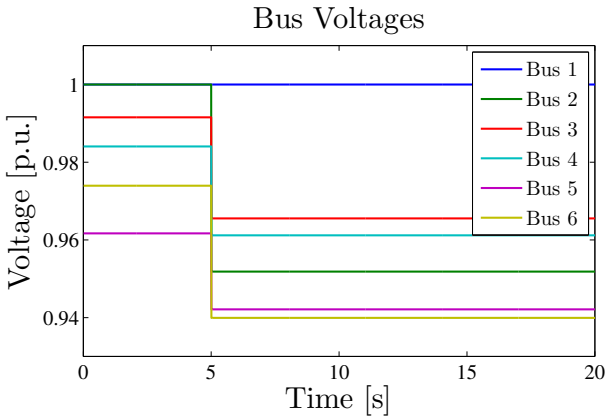


Figure 3.5: Base Case without Control

#### 3.5.3.2 Reactive Power Control on Bus 6

Figure 3.6a shows the bus voltages for the unconstrained case with coordination of the DERs on only bus 6. The DERs inject 0.1851 p.u. of reactive power to return bus 6 to its pre-contingency value. The impact of the unconstrained case is significant. Every bus is within specifications and buses 3 and 5 recover to within 3% of their original values.

Figure 3.6b shows the bus voltages for the constrained case with coordination of the DERs on bus 6. The resources on bus 6 reach their network capacity of 0.11 p.u. immediately. The change in reactive power consumption on bus 6 proves to be enough to return all of the buses within specification,

although bus 5 has a marginally acceptable voltage reading at 0.9497 p.u. due to its low sensitivity to bus 6.

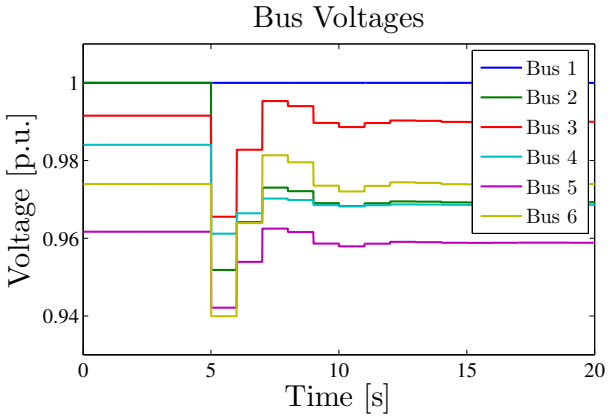


(a) Unconstrained Case

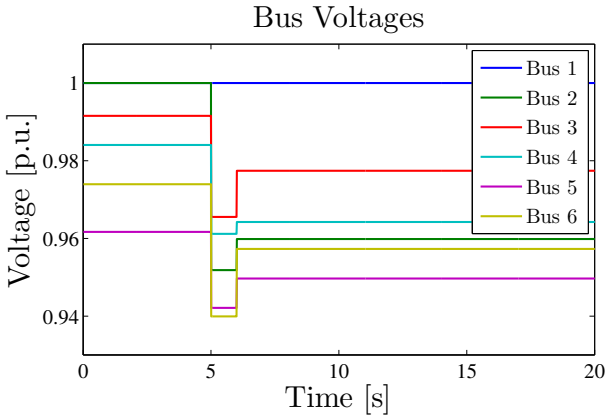


(b) Constrained Case

Figure 3.6: Coordination Control on Bus 6

#### 3.5.3.3 Reactive Power Control on All Load Buses

Figure 3.7a shows the system response to the coordination of the DERs on all of the load buses for the unconstrained case. Every load bus was able to fully recover or return to approximately its pre-contingency value. The amounts of reactive power injected into the network by the DERs on bus 4 and bus 6 are high at 0.2592 p.u. and 0.1125 p.u., respectively. The reactive power injected on bus 5 was relatively low at 0.0301 p.u.

Figure 3.7b shows the voltage waveforms for the constrained case. Unlike the constrained case with reactive power support solely on bus 6, all of the bus

voltages are well within specifications. From the observed node contributions in the unconstrained case, it is clear that the DERs on bus 4 and bus 6 will operate at their capacities. Bus 5 injects more reactive power to compensate for buses 4 and 5 reaching their limits and increases its contribution to 0.0804 p.u. Notice that bus 5 has the ability to produce more reactive power and has the lowest bus voltage. A possible method for future control strategies is that the reference voltage on this bus could be increased to reduce the voltage error on other buses with high sensitivities to it. Another observation is that the reactive power injected by bus 4 in the unconstrained case is 236% that of the constrained case, but the bus voltage is only 1.18% less than the nominal value. This should be considered for strategies that also incorporate active power support because the system may benefit from a larger injection of active power than reactive power.

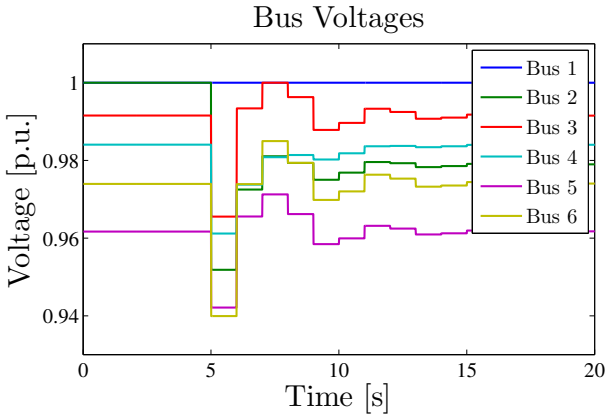


(a) Unconstrained Case

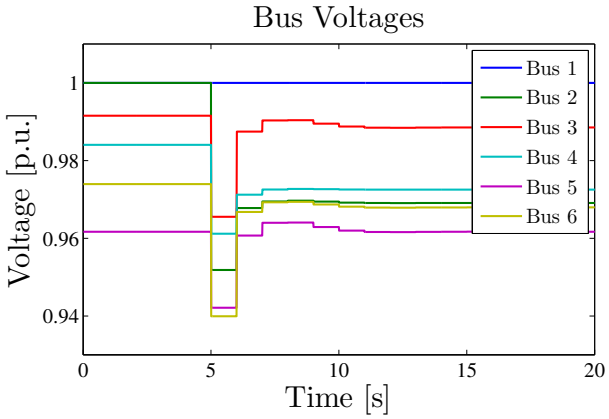


(b) Constrained Case

Figure 3.7: Coordination Control on all Load Buses

#### 3.5.3.4 Algorithm Performance

The evolution of the nodes is shown in Fig. 3.8a. The eigenvalues for the state transition matrix $P_c$ are $\sigma(P_c) = \{1, 0.4279, 0.333, -0.260\}$. The second largest eigenvalue for this system is small and the system converges quickly to the limit.

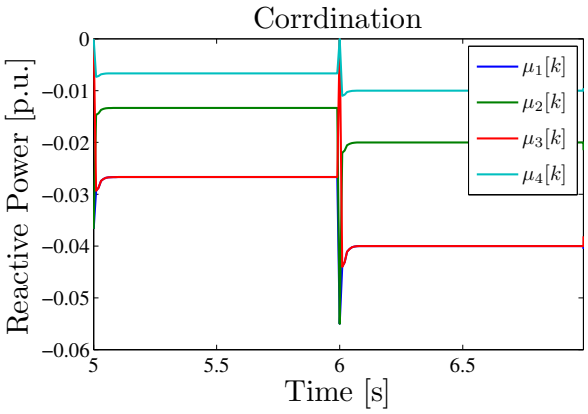


(a) Non-Adaptive Fair Splitting Algorithm

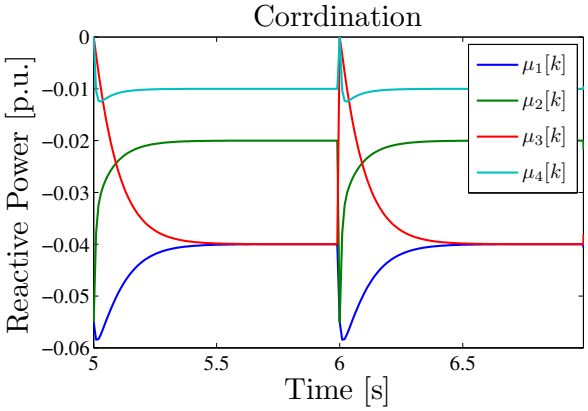


(b) Adaptive Fair Splitting Algorithm

Figure 3.8: Algorithm Convergence

There is another algorithm, the adaptive fair splitting algorithm, discussed in [4] that has similar results and converges to the same values as shown in Fig. 3.8b. This method modifies the state transition matrix weights to create $\bar{P}_c$. A possible control strategy is that if the original $P_c$ is defined such that the second largest eigenvalue $|\lambda_2|$ is large, then an optimized $\bar{P}_c$ may improve the convergence rate of the algorithm by reducing the magnitude of $\lambda_2$. Additionally, one can compute $\bar{P}_c$ optimized to converge to a desired $\bar{\pi}$.

## 3.6 Chapter Summary

In this chapter a localized controller was developed and demonstrated. This is not considered to be a centralized control strategy since the controller has limited measurements and does not consider the voltage profile associated with large radial networks. As a result, this method would not be preferred for networks with large voltage drops from the feeder to the end of the sublaterals. However, this control scheme would be valid for small systems solving resource allocation where operating conditions have minimal fluctuations, i.e., a small neighborhood or DERs on a single distribution system bus.

# Chapter 4

# DISTRIBUTED ALGORITHM FOR DECENTRALIZED VOLTAGE CONTROL

## 4.1 Introduction

The general form of the distributed algorithm for voltage control using nonnegative matrices and the notion of a parametrized matrix were introduced in [4]. The algorithm presented in this chapter extends these results through an adaptive parametrization of the transition matrix. In a power system, the under-voltages and over-voltages are controlled by injecting power or adding load, respectively. As previously discussed, the distributed algorithms require a nonnegative transition matrix; as well, all of the components of $\pi[k]$ must be strictly nonnegative or nonpositive, to ensure convergence. This implies that the under-voltage and over-voltage limits must be handled independently from one another due to the sign difference associated with the reactive power support needed to correct the limit violations. The final solution is the result of the two cases superimposed.

In the proposed strategy, the bus voltages are measured and the algorithm is initialized at steps $r = \{1, 2, \dots\}$. The distributed algorithm is allotted $k$ steps between $r$ and $r + 1$ to converge. Within the interval $(r, r + 1)$, the first $\lfloor k/2 \rfloor$ steps compute the unconstrained resource allocations to correct for the limit violations. The second half of the interval modifies these results to account for capacity constraints. Figure 4.1 illustrates the sequence of events for the algorithm.

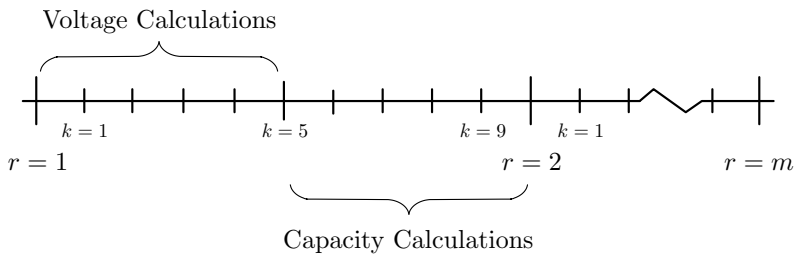


Figure 4.1: Time Scales

## 4.2 Network Communication

Distribution networks are largely radial, with one or more laterals connected to a feeder and several sublaterals branching from the mains. Each system bus is considered to be a node in the representative graph of the network. The communication links between the buses are equivalent to the directed or undirected edges connecting the nodes (refer to Chapter 2). The only exception is the feeder, which will be considered the system slack bus for the power flow calculations. The feeder is essentially an infinite bus whose voltage remains unaffected by the varying loads in the distribution network. Thus, the feeder is not controllable and will not participate in the coordination algorithm. Without loss of generality, it is assumed that every bus in the network can provide reactive power support for voltage control. However, if a particular node cannot provide reactive power support, its capacities will reflect this by assuming that the node is permanently incapacitated. This ensures that the network communication is not restricted by any one node's inability to contribute resources.

Three communication structures will be considered. The first assumes that the nodes are randomly connected and the communication network is independent of physical locations and limitations. The second reflects the physical structure of the distribution network such that there is an undirected communication link for every transmission line in the system. The final configuration modifies the second with transition weights that are biased relative to bus sensitivities.

### 4.2.1 Randomly Connected Graph

The first communication structure randomly creates communication links between all of the nodes, where $a_{ij}$ represents the connection from node $i$ to node $j$. The final graph of the network is required to be strongly connected and aperiodic. As defined in Chapter 2, a graph is strongly connected if for all nodes $i$ and $j$, there exists a path from $i$ to $j$ and $j$ to $i$. Aperiodicity implies that the path and the finite number of steps to travel from $i$ to $j$ is not deterministic.

To create the transition matrix $P_0 \in \mathbb{R}^{n\times n}$, an adjacency matrix $A \in \mathbb{R}^{n\times n}$ is randomly generated. A sufficient condition for aperiodicity is to set $diag\,(A) = [1,\, 1\, \ldots,\, 1]'$, which is equivalent to self-loops on every node. If the resulting graph is strongly connected, then the entries of $P_0$ are given by

$$p_{ij} = \frac{a_{ji}}{\sum_{i=1}^{n} a_{ji}} \quad \forall j. \tag{4.1}$$

Otherwise, a new adjacency matrix will be generated until a strongly connected graph is produced. The transition matrix, $\bar{P} \in \mathbb{R}^{n\times n}$, required for the parametrized $P_0$ is given by

$$\bar{p}_{ij} = \begin{cases} 0 & i = j \\ \frac{a_{ji}}{\sum_{j\neq i} a_{ji}} & i \neq j \end{cases}, \quad \forall j. \tag{4.2}$$

The transition matrices $P_0$ and $\bar{P}$ are column stochastic to ensure that the largest eigenvalue is $\lambda = 1$. The aperiodic and strongly connected requirements on $P_0$ guarantee that this eigenvalue is unique.

### 4.2.2 Network Structure with Even Splitting

The simplest communication network is assumed to have bi-directional communication links that coincide with the transmission lines. In a power system, buses that are directly connected have the highest sensitivities to one another, i.e., this implies that limit violations are localized to specific regions of the network. This method ensures that information is exchanged between neighboring nodes and the steady-state solution for the distributed algorithm will converge around the desired regions.

Let $Y^{-} \in \mathbb{R}^{n\times n}$ be defined as the admittance matrix with the row and

column associated with the system slack bus omitted. Then it follows that the adjacency matrix $A \in \mathbb{R}^{n\times n}$ is defined as the incidence matrix of $Y^-$. The transition matrices $P_0 \in \mathbb{R}^{n\times n}$ and $\bar{P} \in \mathbb{R}^{n\times n}$ are computed with (4.1) and (4.2), respectively.

### 4.2.3 Network Structure with Biased Weights

The previous method developed a transition matrix with equal splitting on the nonzero column entries. This method proposes a transition matrix that has the same adjacency matrix from the even splitting strategy, but biases the transition rates according to bus sensitivities. It can be assumed that the voltage sensitivities of any given bus to changes in reactive power from their neighbors are available through an initialization procedure [2].

The relationship of changes to power relative to changes in bus voltages and phase angles is given by

$$\begin{bmatrix} \Delta P \\ \Delta Q \end{bmatrix} = \begin{bmatrix} \frac{\partial P}{\partial \theta} & \frac{\partial P}{\partial V} \\ \frac{\partial Q}{\partial \theta} & \frac{\partial Q}{\partial V} \end{bmatrix} \begin{bmatrix} \Delta \theta \\ \Delta V \end{bmatrix}. \tag{4.3}$$

Note that $\partial P/\partial\theta\Delta\theta \gg \partial P/\partial V\Delta V$ and $\partial Q/\partial\theta\Delta\theta \ll \partial Q/\partial V\Delta V$ [10]. Given this fact, the decoupled power flow equations assume that $\partial P/\partial V \approx 0$ and $\partial Q/\partial\theta \approx 0$ and the following result is obtained

$$\Delta P = \frac{\partial P}{\partial \theta}\Delta\theta \tag{4.4}$$

$$\Delta Q = \frac{\partial Q}{\partial V}\Delta V. \tag{4.5}$$

The bus voltage sensitivities to changes in reactive power are determined by

$$\begin{aligned} S &= \left[\frac{\partial Q}{\partial V}\right]^{-1} \\ &\approx -\text{imag}\left(Y^-\right)^{-1}. \end{aligned} \tag{4.6}$$

Let the neighbors of node $j$ be defined as the set

$$\mathcal{N}_j := \{i \,|\, \text{node } i \text{ communicates with node } j\}. \tag{4.7}$$

The approximation of $S^{-1}$ in (4.6) results in a sparse symmetric matrix and

$S$ will be a full symmetric matrix that is strictly positive. However, the nodes are only aware of the values of $S_{ji}$ corresponding to their neighbors. They will never be completely aware of every entry in $S$ or the size of the network without implementing a centralized control strategy. The modified sensitivity matrix $\bar{S} \in \mathbb{R}^{n \times n}$ is given by

$$\bar{S}_{ji} = \begin{cases} S_{ji} & i \in \{\mathcal{N}_j \cup j\} \\ 0 & o.w. \end{cases} \quad \forall j. \tag{4.8}$$

The transition matrix $P_0 \in \mathbb{R}^{n \times n}$ is a column stochastic matrix whose transition weights are biased relative to the voltage sensitivities in $\bar{S}$. The components of $P_0$ are calculated by the following

$$p_{ij} = \frac{\bar{S}_{ji}}{\sum_{i \in \{\mathcal{N}_j \cup j\}} \bar{S}_{ji}} \quad \forall j. \tag{4.9}$$

The entries of the column stochastic transition matrix $\bar{P} \in \mathbb{R}^{n \times n}$ used in the adaptive algorithms are given by

$$\bar{P}_{ij} = \begin{cases} \frac{\bar{S}_{ji}}{\sum_{i \in \mathcal{N}_j} \bar{S}_{ji}} & i \neq j \\ 0 & o.w. \end{cases} \quad \forall j. \tag{4.10}$$

The remainder of this thesis assumes that the transition matrix is defined by this method.

## 4.3 Initialization

At each interval $r$, the algorithm begins with an initialization step where the nodes must simultaneously estimate the amount of reactive power support needed to return the bus voltages to their specified operating conditions of 1 p.u. $\pm 5\%$. The underlying principle of this control technique is that the system adds or removes mass at each step $r$, and the distributed algorithm allocates this mass relative to the estimated voltages and node capacities. The coordination of the nodes is required to converge to a feasible solution in an environment with limited knowledge of the global network. Each node has access to its current values and the voltage sensitivities of their neighbors belonging to the set $\mathcal{N}_j$.

The power losses on the transmission lines are small enough that the limit violations are localized to different regions of the network, e.g., a bus experiencing an over-voltage cannot have a neighbor with an under-voltage. Thus, the nodes can assume that their neighbors experience conditions similar to their own. The entries in the sensitivity matrix computed in (4.6) are strictly positive, so any estimation will be inaccurate in a decentralized strategy because the nodes cannot account every node that has an impact on its final value. During initialization the nodes assume that

$$\Delta V_j \approx \Delta V_i \quad \forall i \in \mathcal{N}_j \tag{4.11}$$

$$\Delta Q_j \approx \Delta Q_j \quad \forall i \in \mathcal{N}_j \tag{4.12}$$

$$\frac{\partial V_j}{\partial Q_j} \approx \frac{\partial V_j}{\partial Q_i} \quad \forall i \in \mathcal{N}_j. \tag{4.13}$$

There will be a certain amount of error introduced from these assumptions. Fortunately, an over-estimation enables the system to reach acceptable operating conditions faster and account for some of the reactive power support provided by the nodes they are unaware of.

The initialization procedure at each step $r$ can be summarized as the algorithm computes an estimated $\pi_j[0]$ such that $0.95 \leq V_j^r + \Delta V_j^r \leq 1.05$. To correct for the under-voltages, $\pi_j[0] \geq 0$ so that reactive power is injected into the system and is given by

$$\pi_j[0] = \begin{cases} \frac{0.95 - V_j^r}{\bar{S}_{jj} n_j} & V_j^r \leq 0.95 \\ 0 & o.w. \end{cases} \quad \forall j, \tag{4.14}$$

where $n_j$ is the number of elements in the set $\{\mathcal{N}_j \cup j\}$ and averages the calculated self contributions of node $j$ relative to the assumed values of its neighbors. Similarly, to correct for the over-voltages, $\pi_j[0] \leq 0$ will add reactive power loads to the network and lower bus voltages. $\pi_j[0]$ is defined as

$$\pi_j[0] = \begin{cases} \frac{1.05 - V_j^r}{\bar{S}_{jj} n_j} & V_j^r > 1.05 \\ 0 & o.w. \end{cases} \quad \forall j. \tag{4.15}$$

Notice that the sign of the requested $\pi_j[0]$ depends on the limit violation that is being corrected.

### 4.3.1 Propagation of Convergence Errors

The nodes should ideally converge to a feasible solution within the $k$ iterations between step $r$ and $r+1$, but this is not always the case. The slight capacity violations carried over from the previous interval are accounted for in the initialization step to prevent a cascading capacity constraint error. The difference in capacities is given by

$$\pi_j^{error} = \begin{cases} \pi_j^{max} - \pi_j^{net} & \pi_j^{net} > \pi_j^{max} \\ -\pi_j^{max} - \pi_j^{net} & \pi_j^{net} < -\pi_j^{max} \end{cases} \quad \forall j, \tag{4.16}$$

where $\pi_j^{net}$ is the collective reactive power support provided by the nodes from prior steps. When $\pi_j^{error}$ is positive, it is added to the results in (4.14). Otherwise if $\pi_j^{error}$ is negative, it is summed with the result in (4.15).

## 4.4 Under-Voltage Algorithm

The under-voltage algorithm computes reactive power support exclusively for lower limit violations. If an under-voltage exists, then the required injections are determined to clear the violation. The algorithm consists of two parts that function in series. First, the unconstrained reactive power injections are assigned according to estimated bus voltages. Second, the current results are adjusted so that the node capacities are adhered to.

The parametrized column stochastic transition matrix $P_0$ is given by

$$P_0 = \bar{P}\Delta + (I - \Delta), \tag{4.17}$$

where $\Delta = diag(\delta_1, \delta_2, \ldots, \delta_n)$ with $\delta_j \in [0, 1]$ $\forall j$, and $\bar{P}$ is a column stochastic matrix previously discussed with zero entries on the diagonal.

Given that $P_0$ has been properly defined, there exists a unique distribution such that $\pi = P_0\pi$. However, the equilibrium values of $\pi$ may not distribute reactive power in such a way that the bus voltages meet their operating requirements. By properly controlling the $\delta_j$'s, the proposed algorithm can dynamically control the invariant distribution of $P_0$.

At each time step $k$, the algorithm adjusts the values of the $\delta_j$'s so that the next iteration uses the modified parametrized matrix

$$P[k+1] = \bar{P}\Delta[k+1] + (I - \Delta[k+1]), \tag{4.18}$$

where $[\delta_1[0], \delta_2[0], \ldots, \delta_n[0]]' = \mathbf{1} - diag(P)$ and $P[0] = P_0$.

### 4.4.1 Adaptive Node Voltage Criteria

The first half of the algorithm determines the $p_{jj}$ terms of the transition matrix according to the estimated bus voltages for step $r+1$. Consider the column vector $p_{i1} = [1-\delta_1, \delta_2 p_{12}, \ldots, \delta_n p_{n1}]'$. The value of $\delta_1$ dictates the behavior of the node. For example, node 1 becomes an absorbing state when $\delta_1 = 0$ because any mass sent to node 1 will remain there. Whereas if $\delta_1 = 1$, node 1 will shed its incremental mass.

Let $V_j^r$ be the measured voltage at bus $j$ at step $r$. Given global knowledge of the system, the bus voltage at step $r+1$ can be approximated by (4.5) with

$$\begin{aligned} V_j^{r+1} &= V_j^r + \Delta V_j^r \\ &= V_j^r + \sum_i \frac{\partial V_j}{\partial Q_i}\pi_i. \end{aligned} \tag{4.19}$$

In the decentralized scheme, the nodes only have access to the sensitivities and incremental loads of buses belonging in the set $\{\mathcal{N}_j \cup j\}$. However, limiting (4.19) to the neighbors of $j$ is a sufficient estimation for this control scheme. Therefore, the voltage ratio, $\rho_j[k]$, needed for the update rule at node $j$ is given by

$$\rho_j[k] = \frac{V_j^r + \sum_{i \in \{\mathcal{N}_j \cup j\}} \frac{\partial V_j}{\partial Q_i}\pi_i[k]}{V_j^{nom}}, \tag{4.20}$$

where $V_j^{nom} = 1$ p.u. $\forall j$.

Intuitively, node $j$ requires more reactive power injected if $\rho_j[k] \leq 1$, and will keep more mass for itself on the next iteration. This implies that $\delta_j[k+1] < \delta_j[k]$. Similarly, node $j$ will shed its mass if $\rho_j[k] > 1$ because its incremental voltage is higher than its nominal value. Thus, the update rule used to adjust the behaviors of the nodes is

$$\delta_j[k+1] = \begin{cases} \delta_j[k]\,\rho_j[k] & \rho_j[k] \leq 1 \\ 1-(1-\delta_j[k])\,\frac{1}{\rho_j[k]} & \rho_j[k] > 1 \end{cases}. \tag{4.21}$$

### 4.4.2 Capacity Constraints

The net reactive power consumed or generated is defined as $\pi^{net} \in \mathbb{R}^n$ and is updated prior to each step $r$. The desired result to the the under-voltage scheme is for $\pi_j^{net} + \pi_j[k] \leq \pi_j^{max}$. However, $\pi_j^{net}$ is computed after the under-voltage and the over-voltage algorithms are combined and can take on values in the interval $\left[\pi_j^{min},\, \pi_j^{max}\right]$. For simplicity it is assumed that the capacity limits are $\pm\pi^{max}$.

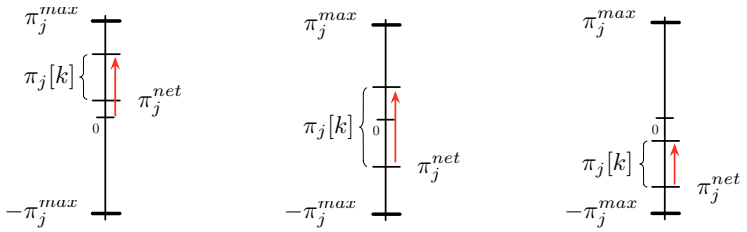


(a) $\pi_j^{net} \geq 0$ (b) $\pi_j \geq -\pi_j^{net}$ (c) $\pi_j < -\pi_j^{net}$

Figure 4.2: Combinations of Net Injections Relative to Capacities

Consider the scenarios in Fig. 4.2. If $\pi_j^{net}$ is nonnegative, then the interval for which the $\pi_j[k]$ is defined is $\left[0,\, \pi_j^{max}\right]$, as denoted in Fig. 4.2a. However, if the current value of $\pi_j^{net}$ is negative, then the maximum injection capacity for the resource no longer has the magnitude $\pi_j^{max}$, as shown in Fig. 4.2b and 4.2c. At each iteration $k$, the computed reactive power injection is shifted according to the current of $\pi_j^{net}$ such that

$$\bar{\pi}_j[k] = \begin{cases} \pi_j[k] + \pi_j^{net} & \pi_j^{net} \geq 0 \\ \pi_j[k] & o.w. \end{cases} \tag{4.22}$$

If $\pi_j^{net}$ is negative, then the new length of the interval is defined as

$$\bar{\pi}_j^{max}[k] = \begin{cases} \pi_j^{max} - \pi_j^{net} & \pi_j^{net} < 0 \\ \pi_j^{max} & o.w. \end{cases} \tag{4.23}$$

The ratio of the current reactive power demanded relative to its capacity is given by

$$\rho_j[k] = \frac{\bar{\pi}_j[k]}{\bar{\pi}_j^{max}[k]} \tag{4.24}$$

and the update equation is

$$\delta_j[k+1] = \begin{cases} \delta_j[k]\,\rho_j[k] & \rho_j[k] \leq 1 \\ 1-(1-\delta_j[k])\,\frac{1}{\rho_j[k]} & \rho_j[k] > 1. \end{cases} \tag{4.25}$$

Therefore, the nodes will adjust their injections until their capacity constraints will be met.

## 4.5 Over-Voltage Algorithm

Similarly to the under-voltage case, the over-voltage algorithm determines the node contributions exclusively for upper limit violations. It differs from the previous in that it computes the amount of load needed to lower bus voltage, so $\pi_j \leq 0\ \forall j$. The quantities defined in the over-voltage case need to be carefully defined such that the parametrized transition matrix presented in (4.9) remains nonnegative. Otherwise, negative entries in the transition matrix will cause the algorithm to diverge.

### 4.5.1 Adaptive Node Voltage Criteria

Initially, the over-voltage algorithm performs the unconstrained resource allocation of the loads during the first $\lfloor k/2 \rfloor$ steps. The ratio of the estimated voltage compared to the nominal, $\rho_j[k]$, is computed from (4.20). If the voltage at node $j$ is high, then $\rho_j[k] > 1$. The node is required to increase its load by reducing the value of $\delta_j$. Otherwise, node $j$ will need to shed its load and $\delta_j$ will become larger. Thus, the update rule for $\delta_j[k+1]$ is described by

$$\delta_j[k+1] = \begin{cases} \delta_j[k]\,\frac{1}{\rho_j[k]} & \rho_j[k] > 1 \\ 1-(1-\delta_j[k])\,\rho_j[k] & \rho_j[k] \leq 1 \end{cases}. \tag{4.26}$$

### 4.5.2 Capacity Constraints

After unconstrained solution relative to bus voltage is determined, the algorithm will adjust the incremental loads to comply with the capacity limits, if necessary. Much like the under-voltage case, the maximum capacity of each node will vary depending on the sign of $\pi_j^{net}$. Figure 4.3 illustrates the possible combinations of $\pi_j^{net}$ and $\pi_j[k]$.

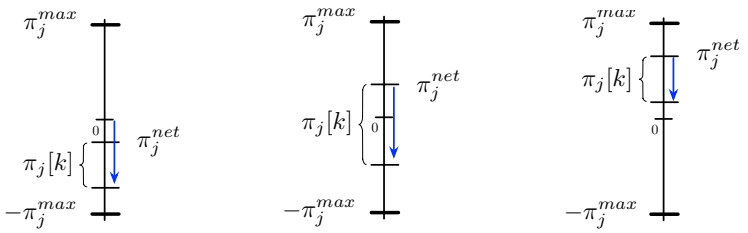


(a) $\pi_j^{net} \leq 0$ (b) $\pi_j \leq -\pi_j^{net}$ (c) $\pi_j > -\pi_j^{net}$

Figure 4.3: Combinations of Net Consumptions Relative to Capacities

Figure 4.3a shows that if the nodes are currently acting as loads, then the maximum capacity for each node remains unchanged. However, the loads carried over from the previous intervals need to be accounted for so that the current incremental injections do not exceed the $\pm\pi^{max}$ capacity specification. Figures 4.3b and 4.3c are the possible situations to consider if $\pi_j^{net} > 0$. As in the previous case, a sign difference causes the magnitude of the maximum capacity constraint to be larger, and the current demand $\pi_j[k]$ does not need to be modified. The relationship of $\pi_j[k]$ to $\pi_j^{net}$ is summarized by

$$\bar{\pi}_j[k] = \begin{cases} \pi_j[k] + \pi_j^{net} & \pi_j^{net} \leq 0 \\ \pi_j[k] & o.w. \end{cases} \tag{4.27}$$

The results for the maximum capacities are given by

$$\bar{\pi}_j^{max}[k] = \begin{cases} -\pi_j^{max} - \pi_j^{net} & \pi_j^{net} > 0 \\ -\pi_j^{max} & o.w. \end{cases} \tag{4.28}$$

The ratio required for the update rule is

$$\rho_j[k] = \frac{\bar{\pi}_j[k]}{\bar{\pi}_j^{max}[k]}. \tag{4.29}$$

When $\rho_j[k]$ is greater than 1, the incremental load will increase the load on bus $j$ beyond its capacity, so the node will shed its load. Otherwise, the nodes can continue to increases their loads to accommodate nodes that have reached their capacities. The update rule for the node capacities is

$$\delta_j[k+1] = \begin{cases} \delta_j[k]\,\rho_j[k] & \rho_j[k] \leq 1 \\ 1-(1-\delta_j[k])\,\frac{1}{\rho_j[k]} & \rho_j[k] > 1. \end{cases} \tag{4.30}$$

Notice that $\Delta$ will always converge to an identity matrix for both the under-voltage and the over-voltage algorithms. If the solution obtained using the voltage criteria meets the capacity constraints, it will remain unchanged because $\Delta$ is carried over from the previous half of the algorithm.

## 4.6 8 Bus Feeder Example

The following example uses the 8 bus distribution network shown in Fig. 4.4a. The feeder is considered the system slack bus, and the remaining seven nodes are able to provide reactive power support. Figure 4.4b is the equivalent graph for the communication layer of the network.

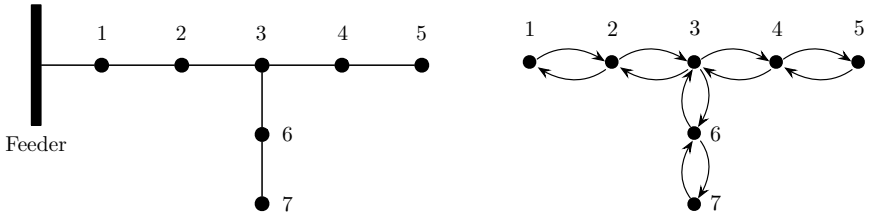


(a) Topology (b) Communication Network

Figure 4.4: 8 Bus Distribution Network

The maximum capacities for the nodes are $\pi^{max} = [1.0,\ 0.7,\ 0.625,\ 0.5,\ \ldots\ 0.425,\ 0.65,\ 0.625]'$ p.u. The sensitivity matrix $\bar{S}$ computed from (4.8) is

given by

$$\bar{S} = \begin{bmatrix} 0.5384 & 0.5388 & 0 & 0 & 0 & 0 & 0 \\ 0.5388 & 1.3183 & 1.3201 & 0 & 0 & 0 & 0 \\ 0 & 1.3201 & 2.8303 & 2.8313 & 0 & 2.8308 & 0 \\ 0 & 0 & 2.8313 & 2.6888 & 3.6897 & 0 & 0 \\ 0 & 0 & 0 & 3.6897 & 5.3016 & 0 & 0 \\ 0 & 0 & 2.8308 & 0 & 0 & 3.5155 & 3.5158 \\ 0 & 0 & 0 & 0 & 0 & 3.5158 & 4.4361 \end{bmatrix} \times 10^{-2}. \tag{4.31}$$

The initial biased transition matrix computed from (4.9) is given by

$$P_0 = \begin{bmatrix} 0.4998 & 0.1696 & 0 & 0 & 0 & 0 & 0 \\ 0.5002 & 0.4149 & 0.1345 & 0 & 0 & 0 & 0 \\ 0 & 0.4155 & 0.2885 & 0.2773 & 0 & 0.2870 & 0 \\ 0 & 0 & 0.2885 & 0.3613 & 0.4104 & 0 & 0 \\ 0 & 0 & 0 & 0.3614 & 0.5896 & 0 & 0 \\ 0 & 0 & 0.2885 & 0 & 0 & 0.3565 & 0.4421 \\ 0 & 0 & 0 & 0 & 0 & 0.3565 & 0.5579 \end{bmatrix} \tag{4.32}$$

and the transition matrix from (4.10) is given by

$$\bar{P} = \begin{bmatrix} 0 & 0.2899 & 0 & 0 & 0 & 0 & 0 \\ 1 & 0 & 0.1891 & 0 & 0 & 0 & 0 \\ 0 & 0.7101 & 0 & 0.4342 & 0 & 0.4460 & 0 \\ 0 & 0 & 0.4055 & 0 & 1 & 0 & 0 \\ 0 & 0 & 0 & 0.5658 & 0 & 0 & 0 \\ 0 & 0 & 0.4054 & 0 & 0 & 0 & 1 \\ 0 & 0 & 0 & 0 & 0 & 0.5540 & 0 \end{bmatrix}. \tag{4.33}$$

The initial diagonal entries of $\Delta$ from (4.18) are $\delta[k] = [0.5002, 0.5851, \ldots$ 0.7116, 0.6387, 0.4104, 0.6435, 0.4421].

The operating requirements for this system are that the bus voltages must be within $\pm 5\%$ of the nominal 1 p.u. voltage. To show the distributed algorithm's ability to correct for an over-voltage, the feeder voltage is set to 1.08 p.u. This causes an over-voltage on bus 1 of 1.0642 p.u. Two versions of the distributed algorithm are demonstrated. The first results only correct

for the over-voltage. The second run combines the methods described in Sections 4.4 and 4.5 for the finalized version of the distributed voltage control algorithm.

The results in Fig. 4.5 are the system's responses for the constrained over-voltage case. The system immediately responds to the over-voltage by increasing the reactive power load on every bus. The final voltage measurement at bus 1 is 1.0501 p.u. and is well within acceptable tolerances. However, the voltages at buses 4, 5, and 7 violate the lower bound of the voltage limits with values of 0.9354, 0.9354, and 0.9466, respectively.

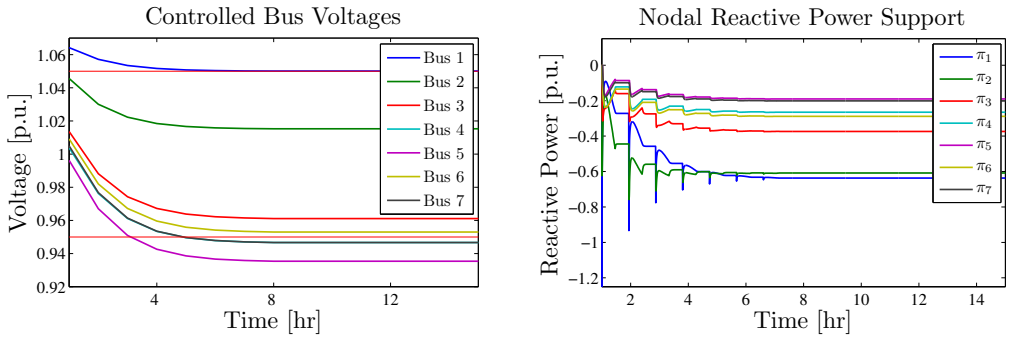


(a) Bus Voltages (b) Reactive Power Support

Figure 4.5: Algorithm with Respect to Over-Voltage

Figure 4.6 shows the results for the combined under-voltage and over-voltage components of the distributed algorithm. As in the previous case, the over-voltage on bus 1 is immediately corrected. Once the under-voltage occurs on bus 5, the under-voltage algorithm starts to inject reactive power on buses 4, 5, and 7. Nodes 1, 2, and 3 respond to this by increasing their loads.

The final results for the bus voltages and node contributions from the two cases are listed in Tables 4.1 and 4.2, respectively. The parallel distributed algorithm was able to correct for both types of voltage limit violations and meet the desired system operational requirements within $\pm 0.001$ p.u.

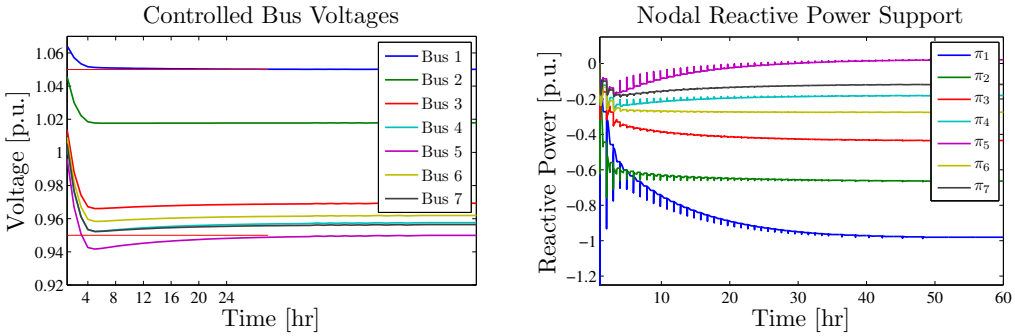


(a) Bus Voltages

(b) Reactive Power Support

Figure 4.6: Parallel Algorithm

Table 4.1: Steady-State Voltages

| Bus | Without Support | Over-Voltage Algorithm | Parallel Algorithms |
|---|---|---|---|
| 1 | 1.0642 | 1.0501 | 1.0501 |
| 2 | 1.0456 | 1.0152 | 1.0178 |
| 3 | 1.0136 | 0.9611 | 0.9693 |
| 4 | 1.0038 | 0.9466 | 0.9576 |
| 5 | 0.9962 | 0.9354 | 0.9499 |
| 6 | 1.0091 | 0.9530 | 0.9619 |
| 7 | 1.0049 | 0.9466 | 0.9564 |

Table 4.2: Nodes Value for Reactive Power Support

| Bus | $\pi^{max}$ | Over-Voltage Algorithm | Parallel Algorithms |
|---|---|---|---|
| 1 | $\pm 1$ | -0.6367 | -0.9805 |
| 2 | $\pm 0.700$ | -0.6083 | -0.6634 |
| 3 | $\pm 0.625$ | -0.3736 | -0.4345 |
| 4 | $\pm 0.500$ | -0.2651 | -0.1803 |
| 5 | $\pm 0.425$ | -0.1905 | 0.0208 |
| 6 | $\pm 0.650$ | -0.2886 | -0.2744 |
| 7 | $\pm 0.625$ | -0.2012 | -0.1177 |

## 4.7 Chapter Summary

This chapter develops a distributed voltage control algorithm that corrects for both over-voltages and under-voltages through parallel computations. Additionally, the algorithm is able to converge to solutions that comply with capacity constraints on the nodes. A simple 8 bus example was used to illustrate the ability of the control to correct for an over-voltage. Further applications of the control technique will be presented in a series of case studies later in this thesis.

# Chapter 5

# CASE STUDIES

## 5.1 Introduction

Distribution systems differ dramatically from transmission systems in that their $x/r$ ratio is much lower. This results in bus voltages that are much more sensitive to changes in active power [14, 29]. Given a significant penetration of photovoltaic (PV) installations, the active power injected into the electrical grid can cause over-voltages on buses near the feeder when the incident irradiance peaks midday and the demanded loads are relatively low. The solar decathlon house constructed by the University of Illinois for the 2009 competition is a prime example of a residential PV installation capable of producing positive net power during peak hours of the day [30]. This chapter discusses the potential impacts on bus voltages caused by a high penetration of PV installations similar to that of the University of Illinois' Gable Home.

Three case studies were conducted to illustrate the implementation of the distributed algorithms for voltage control. Each study uses several weather profiles and the same load demand curve. In the first study, the response of an 8 bus system to the different weather profiles is studied. The same set of weather and load profiles are applied to the modified IEEE 123 bus distributed system. Finally, the response of the 123 bus system is studied under a different communication structure with independent clusters of nodes. Additionally for the 123 bus distribution systems, the load profile for plug-in electric hybrid vehicles (PHEV) is applied.

## 5.2 PV Generation for Different Weather Profiles

The simulations have access to six separate weather profiles developed from four different curves fitted to data collected by the University of Nevada in Las Vegas, Nevada during 2007 [31]. Figure 5.1a provides the active power produced by PV systems under nominal conditions on a clear day. Figure 5.1b is the active power generated on a cloudy day with intermittent exposure to sunlight. Figures 5.1c and 5.1d have limited sunlight exposure in the morning and ideal power production during the second half of the day. Assuming that the PV systems experience ideal conditions in the morning and cloud cover in the afternoon, the curves from Fig. 5.1c and 5.1d are reversed.

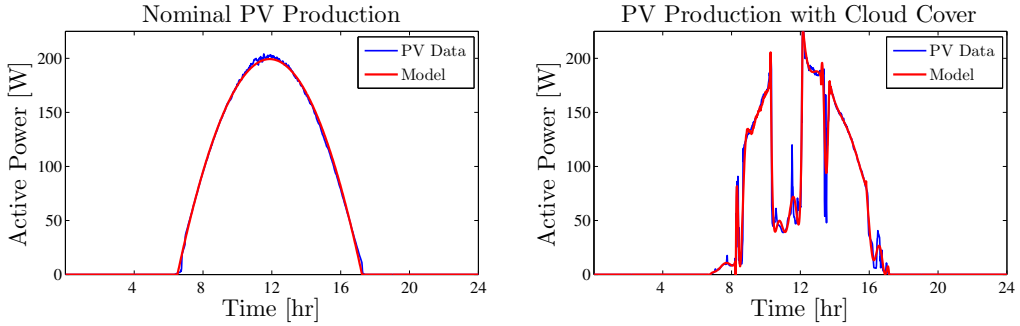


(a) Clear Day (b) Cloud Cover

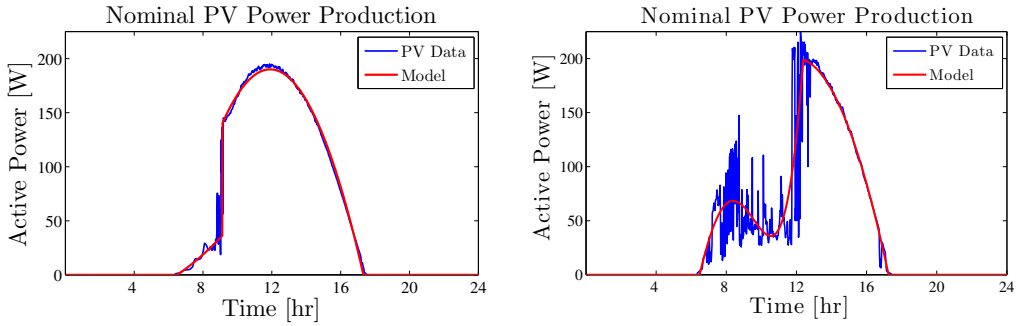


(c) Cloud Cover Early Morning (d) Cloud Cover Half Day

Figure 5.1: PV Profiles

The impact of active power injections from PV systems is best understood when joined with load curves throughout the day. For example, PV power generation peaks around noon, which does not coincide with the peak demand. To account for this phenomena, load data was gathered from the regional transmission organization (RTO) PJM, which offers 18 years of histori-

cal metered data supplied by their electric distribution companies (EDC) [32]. The data itself is sampled every hour of each day of the year. The load profile in Fig. 5.2a was created by fitting a curve to data selected from PJM's 2010 metered historical data for the PS load zone.

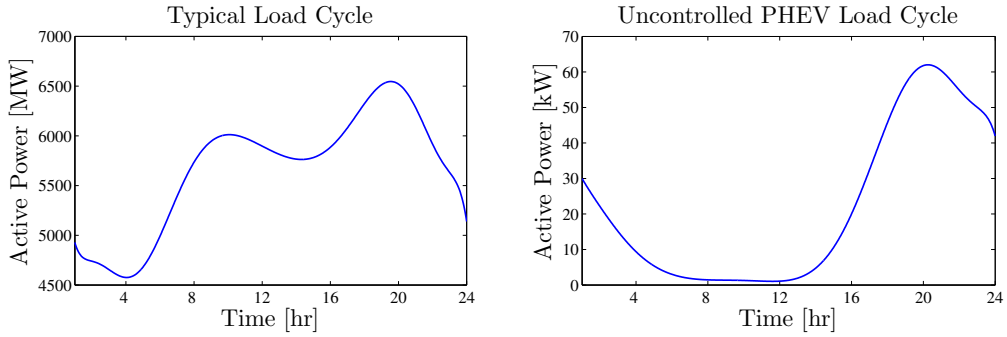


(a) 24 Hour Load Profile (b) PHEV Load Curve

Figure 5.2: Load Curves

It is assumed that the load curve for every bus is a scaled version of the load curve in Fig. 5.2a. Therefore, the load profile in Fig. 5.2a is normalized so that its peak value is 1 and multiplied by the value of the static load at each bus. Figure 5.2b shows the uncontrolled load introduced to the network from PHEVs [6, 7]. In the simulations for the 123 bus network, the curve is normalized to 1 and loads are defined as a maximum additional percentage to the current load, e.g., the current load is 120% of the value that it would be without PHEVs at 8:00 P.M. Additionally, the operational requirements for the voltage on every bus is 1 p.u. $\pm 5\%$.

## 5.3 Constrained 8 Bus Distribution Network

The 8 bus distribution network shown in Fig. 5.3 is used to demonstrate the distributed algorithms for voltage control. The communication structure is a single communicating class that follows the network topology as described in Section 4.2.3. The feeder is considered the slack bus for the system and is assumed to be experiencing an over-voltage of 1.0633 p.u. Typically, a tap-changing under load (TCUL) transformer will react to this violation and adjust the tap to lower the voltage. However, this particular system is configured such that every load bus is within specifications, where the highest

voltage measurement is on bus 1 at 1.05 p.u. and the lowest measured voltage is on bus 5 at 0.95 p.u. The tap ratio is held constant the entire duration of the simulation for several reasons: (i) it is assumed that the ability of the nodes to react to voltage violations is faster than that of the TCUL transformer, (ii) the objective of the case studies is to observe the ability of the distributed algorithms to converge to a solution, and (iii) any changes to the tap position will result in an under-voltage or an over-voltage.

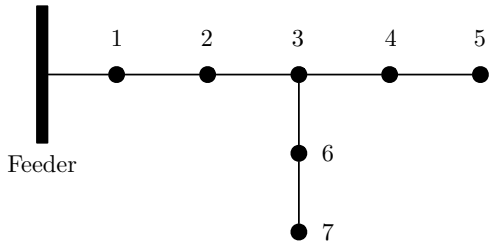


Figure 5.3: 8 Node Distribution Network

The sensitivities of the bus voltages to changes in active and reactive power can by computed from the jacobian used in the Newton-Rhapson power flow method. The bus voltage sensitivities to changes in active power are given by

$$\left[\frac{\partial V_i}{\partial P_j}\right] = \begin{bmatrix} 0.153 & 0.202 & 0.286 & 0.314 & 0.337 & 0.297 & 0.311 \\ 0.157 & 0.380 & 0.585 & 0.655 & 0.712 & 0.613 & 0.648 \\ 0.164 & 0.395 & 1.128 & 1.276 & 1.397 & 1.188 & 1.262 \\ 0.165 & 0.399 & 1.140 & 1.527 & 1.682 & 1.201 & 1.275 \\ 0.167 & 0.402 & 1.150 & 1.540 & 2.227 & 1.210 & 1.285 \\ 0.164 & 0.397 & 1.133 & 1.283 & 1.403 & 1.415 & 1.506 \\ 0.165 & 0.398 & 1.138 & 1.288 & 1.409 & 1.421 & 1.675 \end{bmatrix} \times 10^{-2} \tag{5.1}$$

and bus voltage sensitivities to changes in reactive power are

$$\left[\frac{\partial V_i}{\partial Q_j}\right] = \begin{bmatrix} 0.704 & 0.729 & 0.767 & 0.778 & 0.786 & 0.772 & 0.777 \\ 0.722 & 1.809 & 1.902 & 1.929 & 1.949 & 1.914 & 1.926 \\ 0.751 & 1.881 & 4.062 & 4.121 & 4.163 & 4.088 & 4.114 \\ 0.759 & 1.901 & 4.106 & 5.344 & 5.398 & 4.132 & 4.159 \\ 0.766 & 1.917 & 4.140 & 5.388 & 7.629 & 4.166 & 4.193 \\ 0.755 & 1.890 & 4.082 & 4.142 & 4.183 & 5.021 & 5.054 \\ 0.758 & 1.898 & 4.100 & 4.160 & 4.201 & 5.043 & 6.359 \end{bmatrix} \times 10^{-2}. \tag{5.2}$$

Although the buses are clearly more sensitive to changes in reactive power,

their sensitivities to changes in active power are less than half an order of magnitude. With the system functioning close to its operational limits, the sensitivities suggest that a significant injection of active power can cause an over-voltage. Similarly, the higher sensitivities to changes in reactive power imply that reactive power support to correct limit violations is preferred.

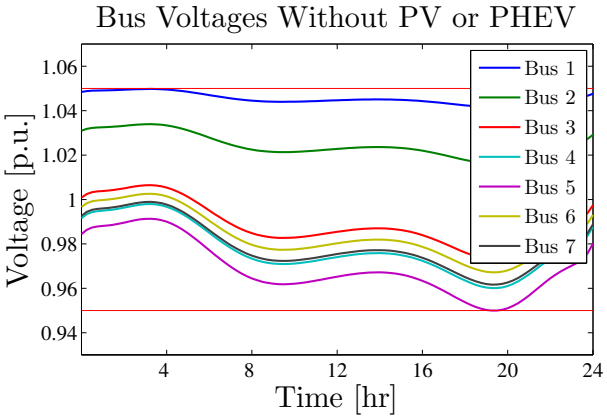


Figure 5.4: Voltage Profile for the 8 Bus Network

The system response to four separate weather conditions was observed. The bus voltages are plotted with and without the distributed voltage control algorithm, as well as the reactive power support provided by the nodes, for each case. Figure 5.4 shows the voltage profile of the 8 bus network with the load curve from Fig. 5.2a applied to the seven load buses. Table 5.1 lists the maximum load, $P_L$ and $Q_L$, and the active power capacities for PV generation, $P_{PV}$, for each node.

Table 5.1: Bus Values

| Bus | $\|V\|$ | $P_L$ | $Q_L$ | $P_{PV}$ | $\pi^{max}$ |
|---|---|---|---|---|---|
| Feeder | 1.063 | - | - | - | - |
| 1 | 1.042 | 0.630 | 0.090 | 0.580 | $\pm$ 0.1 |
| 2 | 1.016 | 0.765 | 0.225 | 0.704 | $\pm$ 0.1 |
| 3 | 0.973 | 0.540 | 0.135 | 0.497 | $\pm$ 0.1 |
| 4 | 0.960 | 1.125 | 0.450 | 1.035 | $\pm$ 0.1 |
| 5 | 0.950 | 0.810 | 0.270 | 0.745 | $\pm$ 0.1 |
| 6 | 0.967 | 0.090 | 0.090 | 0.083 | $\pm$ 0.1 |
| 7 | 0.962 | 0.900 | 0.315 | 0.828 | $\pm$ 0.1 |

It was assumed that the DERs were designed to provided each bus with $\pm 0.1$ p.u. of reactive power support. This creates a situation where the capacity limits will be reached, but the network as a whole will not be significantly constrained. The sampling periods for the presented graphs are listed in Table 5.2. The time constants are slightly arbitrary and will depend on the time constants of the power electronics used to control the DERs. The sampling periods were chosen such that the ability of the control strategy could be demonstrated, while the arrays stored in MATLAB were appropriately sized such that the data could be manipulated and analyzed.

Table 5.2: System Sampling

| Sampled Item | Sample Period |
|---|---|
| Demanded Loads | 15 min |
| Steps | 2.14 min |
| Iterations | 0.85 sec |

## Case 1: Nominal PV Injections

The first case assumes that all of the PV systems are operating under nominal conditions as described by Fig. 5.1a. Without the contributions of the PV systems, the highest voltage occurs in the morning when the loads are lower. As a result, bus 1 initially operates near its upper voltage limit. As the PV resources start to inject active power into the system, an over-voltage occurs at 8:00 A.M. in the uncontrolled voltage response represented in Fig. 5.5a. The PV generation peaks at noon with a maximum combined power injection of 4.471 p.u. and creates an over-voltage of 1.054 p.u. on bus 1.

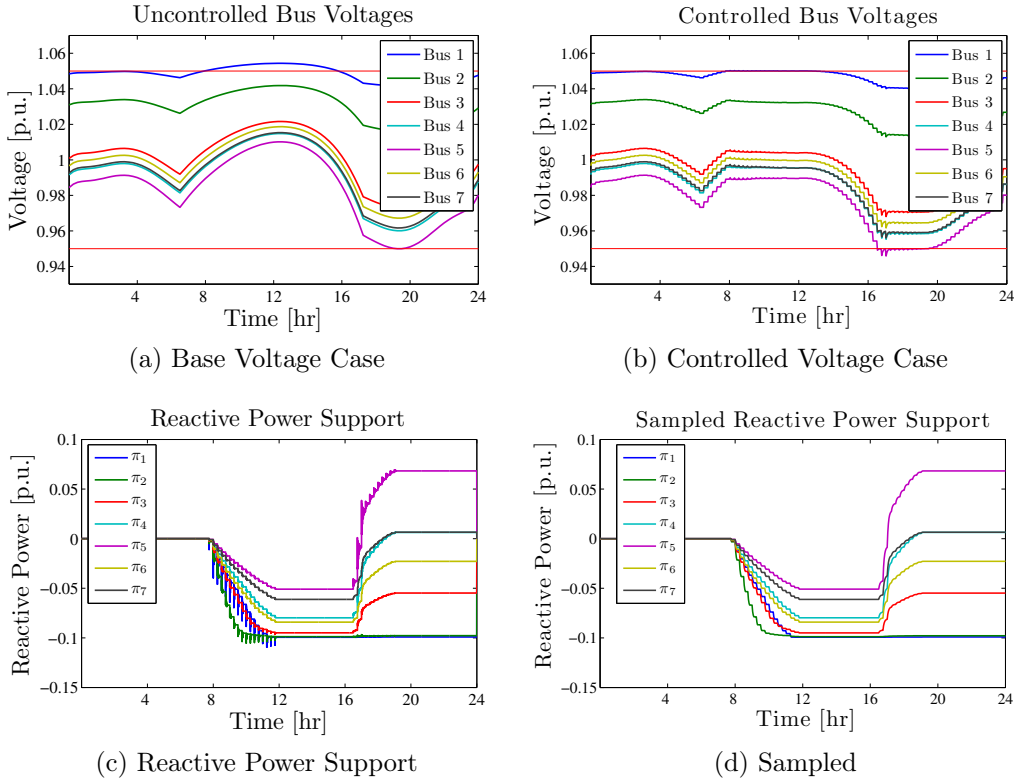


(a) Base Voltage Case

(b) Controlled Voltage Case

(c) Reactive Power Support

(d) Sampled

Figure 5.5: Case 1 for the 8 Node Network

Figures 5.5b and 5.5c are the system responses when the voltage control scheme is implemented. Figure 5.5d shows the final values that are sampled when the distributed algorithm converges. The nodes immediately address the over-voltage from 8:00 A.M. to 4:00 P.M. by consuming reactive power to lower the voltage at bus 1. Node 1 quickly reaches its maximum capacity. Since bus 1 has the highest sensitivities to nodes 2 and 3, the nodes increase their loads to compensate for it. As the active power produced by the PV

systems starts to decrease in the afternoon, the nodes will not adjust their current values until an event triggers them to do so. The additional load introduced by the nodes causes an under-voltage at 4:45 P.M. The buses at the end of the laterals experience significant voltage drops. Node 5 starts to inject reactive power to increase the voltage measurement on bus 5, while nodes 1 and 2 hardly adjust their values. The remaining nodes either change their values to 0, or they reduce their load so that all of the constraints are satisfied.

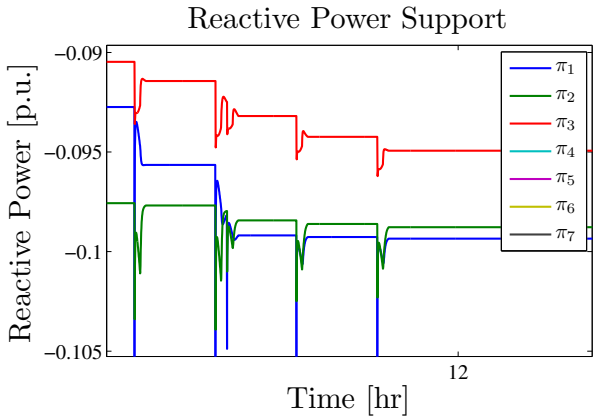


Figure 5.6: Node Capacity Boundaries

Figure 5.6 is a close-up view of the reactive power loads provided by the nodes when the over-voltage happens. The distributed voltage control algorithm does not enforce hard limits, but rather it is designed to converge resource limits as long as the initial request is less than the network capacity. Nodes 1, 2, and 3 have the highest sensitivities to the over-voltage on bus 1, and as a result, they approach their capacity limits.

## Case 2: Morning Cloud Cover

In the second case, the system experiences cloud cover in the morning and ideal sunlight exposure in the afternoon, as described in Fig. 5.1c. Figures 5.7a and 5.7b show the voltage responses with and without control. The primary difference between this case and the previous one is that the active power injections from the PV system have a sudden spike at 9:00 A.M., rather than a steady increase in generation. The sudden over-voltage causes a large jump in Figs. 5.7c and 5.7d. The initial request for the interval beginning

at 9:00 A.M. is $\pi[0] = [-0.1495\,0\,0\,0\,0\,0\,0]'$. The nodes quickly distribute the demand amongst themselves to prevent any capacity violations. Once the algorithm converges to correct for the limit violation at noon, the response of the nodes and bus voltages to the under-voltage at 4:45 P.M. is nearly identical to the first case. The slight differences in the $\pi_j$'s can be explained by the fact that the distributed algorithm is adaptive on the basis of current measurements. Otherwise, the results of the two cases are generally within $\pm 0.002$ p.u. after they converge to correct the over-voltage at noon.

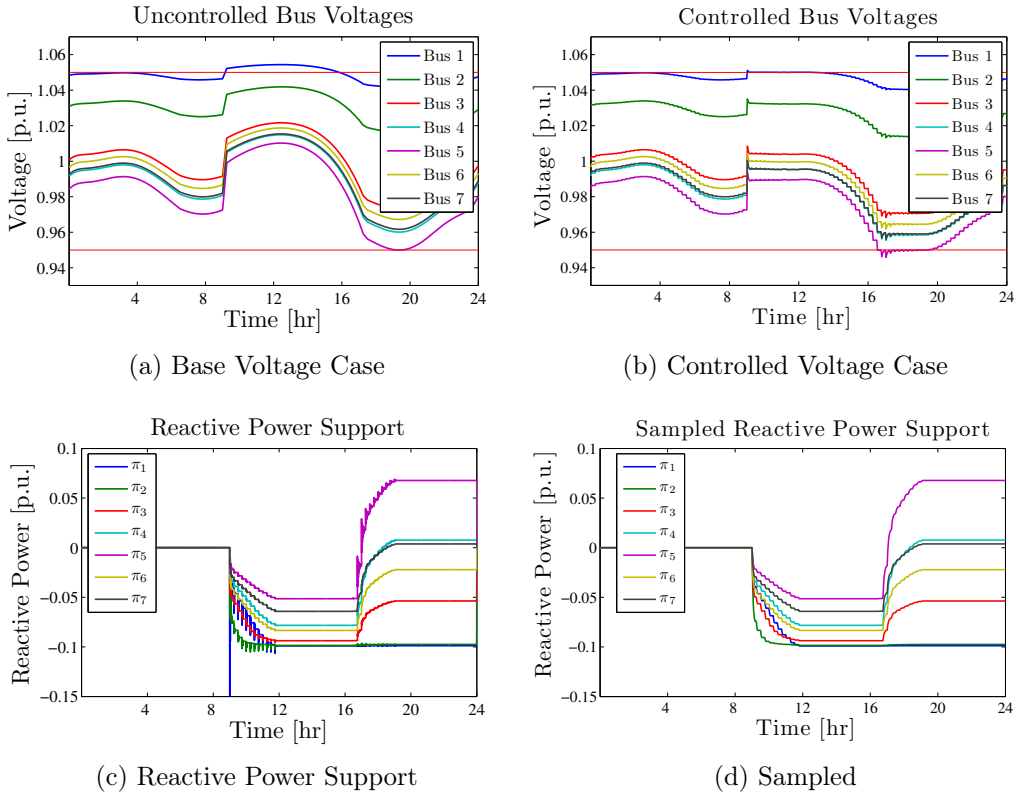


(a) Base Voltage Case

(b) Controlled Voltage Case

(c) Reactive Power Support

(d) Sampled

Figure 5.7: Case 2 for the 8 Node Network

## Case 3: Afternoon Cloud Cover

In the third case, the PV systems encounter ideal sunlight exposure in the morning. However, upon reaching their peak at noon, they experience cloud cover for the rest of the day. This case uses reversal the PV profile shown in Fig. 5.1d where the array for the profile is indexed from its end to its beginning. The results of this case are shown in Figs. 5.8a to 5.8d. Bus

1 experiences an over-voltage from 8:00 A.M. to noon and bus 5 has an under-voltage at 4:45 P.M. due to the added loads to correct for the previous voltage violation. Although the bus voltages are different from the first case, cloud cover has no effect on node contribution if the PV sources reach their maximum outputs.

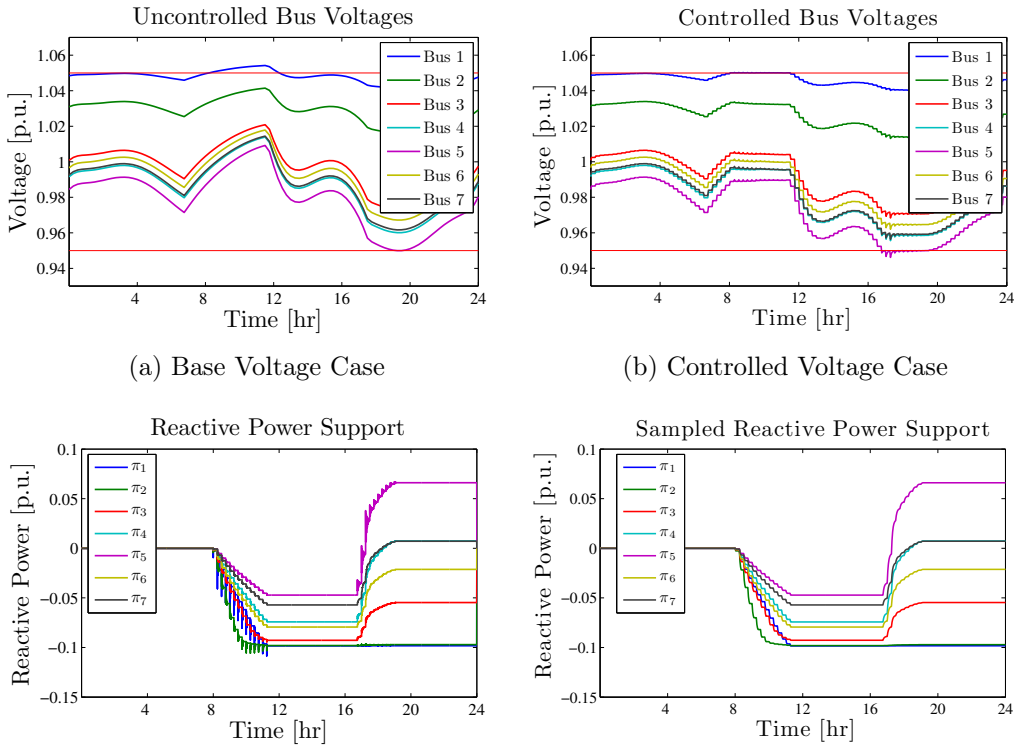


(a) Base Voltage Case

(b) Controlled Voltage Case

(c) Reactive Power Support

(d) Sampled

Figure 5.8: Case 3 for the 8 Node Network

## Case 4: Intermittent Cloud Cover

The PV systems in the final case follow the curve in Fig. 5.1b. Figures 5.9a and 5.9b show the system responses to the sudden changes in active power injected by the PV systems. The nodes react to the first two over-voltages at 8:45 A.M. and noon. The third voltage spike at 1:30 P.M. does not cause an over-voltage since the loads introduced by the nodes are enough to prevent another limit violation. The voltage and node responses to the under-voltage at 4:45 P.M. are similar to the previous cases with subtle differences resulting from the node's response to the over-voltage earlier in the day. The reactive

power support provided by the nodes is shown in Figs. 5.9c and 5.9d.

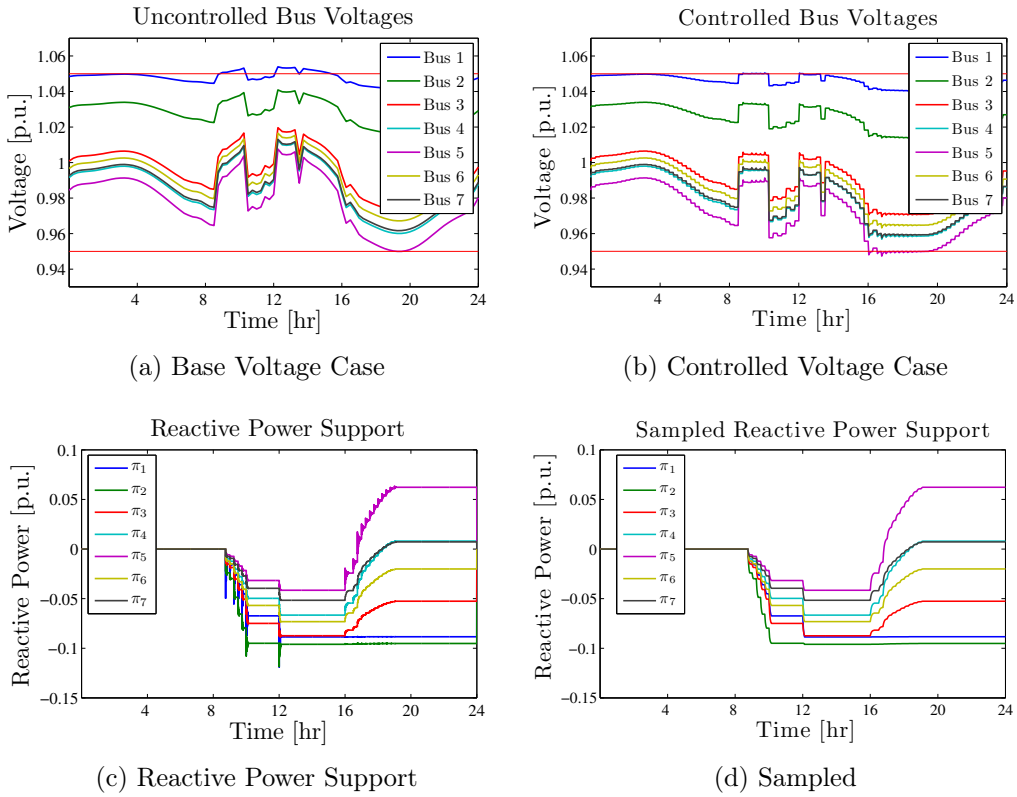


(a) Base Voltage Case

(b) Controlled Voltage Case

(c) Reactive Power Support

(d) Sampled

Figure 5.9: Case 4 for the 8 Node Network

## 5.4 123 Bus Distribution Network

The systems used in the two following case studies in Sections 5.4.1 and 5.4.3 are based on the IEEE 123 bus distribution network from the IEEE PES Distribution System Analysis Subcommittee [33]. The original IEEE 123 bus system model is a three-phase unbalanced network and was modified to be analyzed as a single phase or a three-phase balanced network. The layout of the modified distribution network is pictured in Fig. 5.10.

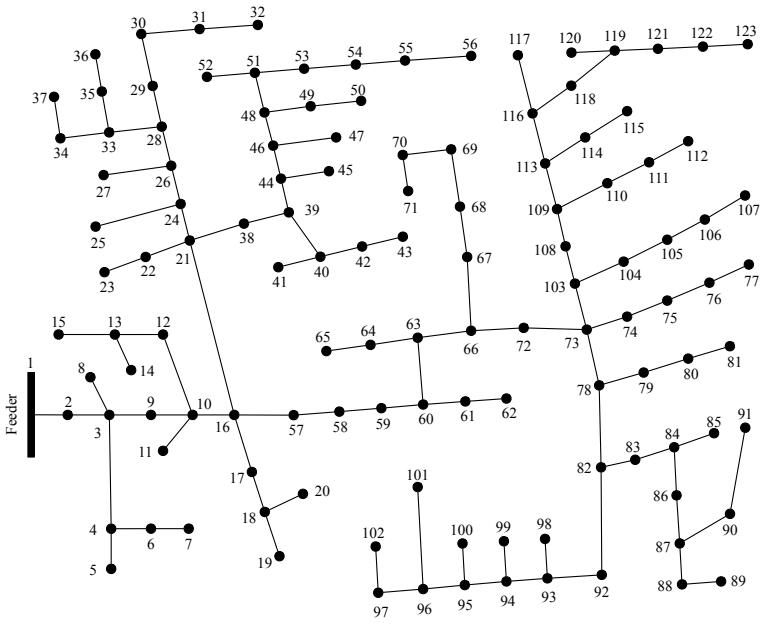


Figure 5.10: 123 Node Distribution Network

The two case studies performed with the 123 bus network only differ by their communication structure. Therefore the time constants used for the simulations are the same and listed in Table 5.3. The sampling time of the iterations for the 123 bus system was reduced from the 8 bus system to allow for more iterations between each step to improve convergence.

Table 5.3: System Sampling

| Sampled Item | Sample Period |
|---|---|
| Demanded Loads | 15 min |
| Steps | 2.14 min |
| Iterations | 0.26 sec |

The voltage magnitudes, maximum load values, maximum active power injections for the PV systems, and maximum loads from the PHEVs are listed in Table B.1. It is assumed that the nodes are designed to provide $\pm 0.4$ p.u. of reactive power. Each of the load buses uses a scaled version of the load profile shown in Fig. 5.2a and the uncontrolled PHEV load curve in Fig. 5.2b. In the proposed 123 bus systems, the feeder voltage is set to 1.0585 p.u. With the tap in the TCUL transformer held constant, the system has a

maximum bus voltage of 1.0498 p.u. and a minimum voltage measurement of 0.9507 p.u. Figure 5.11 shows the system response without active power injections from PV systems, reactive power support from the nodes, or loads from the PHEVs.

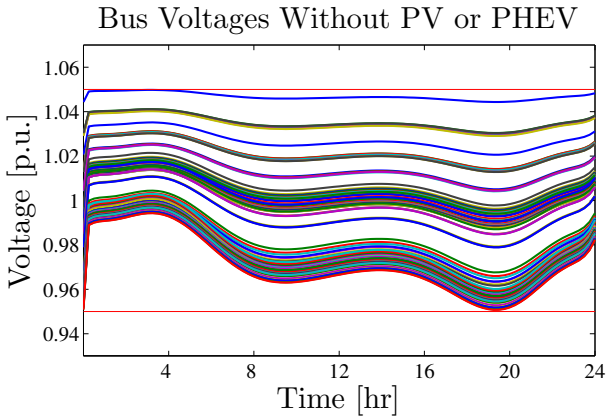


Figure 5.11: Voltage Profile for the 123 Bus Network

### 5.4.1 Constrained 123 Bus Network

Similarly to the case study conducted with the 8 bus distribution network, the 123 bus system is simulated with four separate weather patterns. Each case provides plots for the uncontrolled/controlled voltages and the reactive power contributions of the nodes. In this case study, the communication network is a single communicating class such that the equivalent graph is strongly connected and aperiodic. The communication links follow the network's topology as described in Section 4.2.3.

#### Case 1: Nominal PV Injections

The first case is the system's response under nominal conditions and uses the PV curve in Fig. 5.1a. The uncontrolled bus voltages in Fig. 5.12a show that the active power injected from the PV systems creates over-voltages throughout the system from 8:00 A.M. to 4:00 P.M. The over-voltages peak at noon with a maximum value of 1.0570 p.u. The reactive power support from the nodes is able to correct for the over-voltage violations as shown in 5.12b.

Figures 5.12c and 5.12d are the node responses to the limit violations. There are clearly two events that occur that cause the nodes 69 through 123 to inject reactive power. The first is when the PV systems start prior to noon as several nodes reach their load capacities. During the initialization procedure described in Section 4.3.1, reactive power is injected or consumed to prevent nodes from violating their capacities. The node injections observed are a result of this propagation. The second event happens when the PV systems are no longer producing active power and the load from the PHEVs starts to increase at 5:00 P.M. The nodes are required to inject reaction power to prevent the lower limit voltage violation.

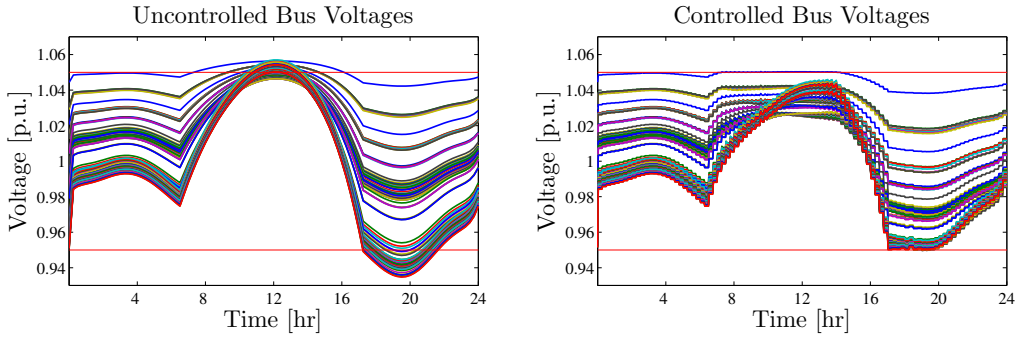


(a) Base Voltage Case

(b) Controlled Voltage Case

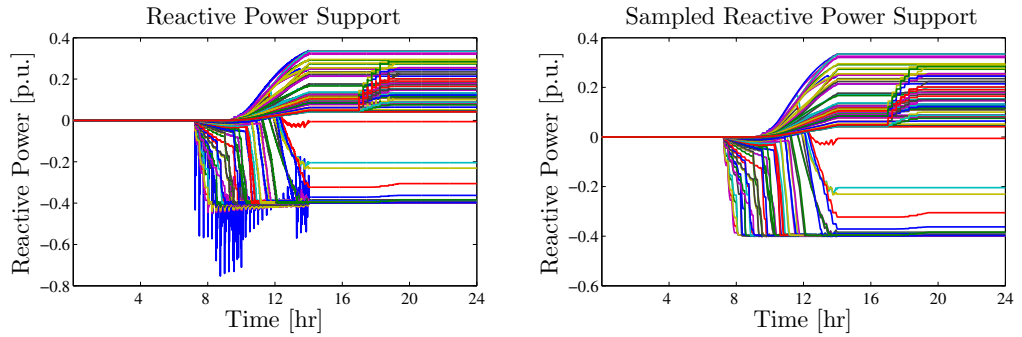


(c) Reactive Power Support

(d) Sampled

Figure 5.12: Case 1 for the 123 Node Network

Nodes 2 through 28 reach their capacities to correct for the over-voltage violation. Figure 5.13 is the close-up of the nodes at their boundaries. The blue represents the evolution of the algorithm for node 2. At the beginning of each step, the initial request for node 2 exceeds its capacity and the load is immediately distributed amongst the nearby nodes. The algorithm converges such that the largest capacity violation is 0.0017 p.u. below the lower bound

of −0.4 p.u, which is an acceptable tolerance.

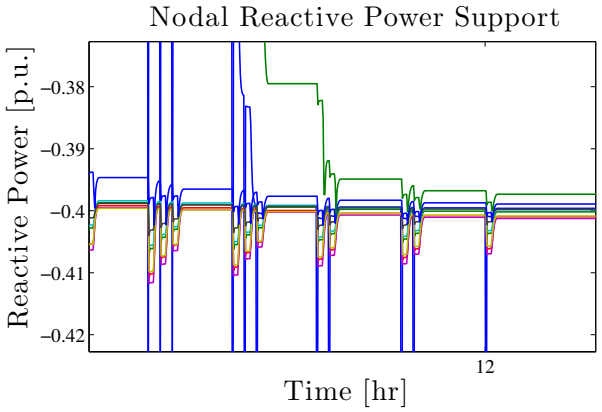


Figure 5.13: Node Capacity Boundaries

## Case 2: Morning Cloud Cover

In the second case, the PV systems experience cloud cover in the morning and have ideal exposure to sunlight after 12:30 P.M. The 123 bus system is large enough that there is a possibility of slight variations in cloud cover across the network. Buses 2 through 65 follow the PV curve in Fig. 5.1c and the remaining buses follow the curve in Fig. 5.1d. Each curve is normalized to 1 and then scaled by the capacities listed in Appendix B. Figure 5.14 shows the net active power injection from the PV systems and captures the combination of the weather profiles.

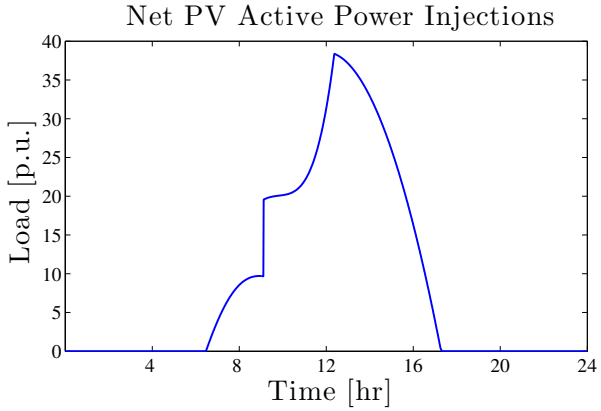


Figure 5.14: Net PV Active Power Resources

The jump in active power production on all of the buses causes an over-

voltage on bus 2 at 9:15 A.M. As in the ideal case, when the PV systems peak around noon, most of the system buses experience an over-voltage with a maximum over-voltage measurement of 1.0572 p.u. Figures 5.15c and 5.16d show that the sudden increase to peak active power generation from the PV systems causes nodes 2 through 26 to reach their capacities faster than in the nominal case. This also explains the reduced reactive power injections from nodes 65 through 123 since the nodes are not required to combat possible capacity violations for such a long period of time. The lower node injections result in a dramatic jump at 5:00 P.M., as opposed the the more subtle curve in the previous case, to prevent the under-voltages in the evening. The voltage results are shown in Figs. 5.15a and 5.15b.

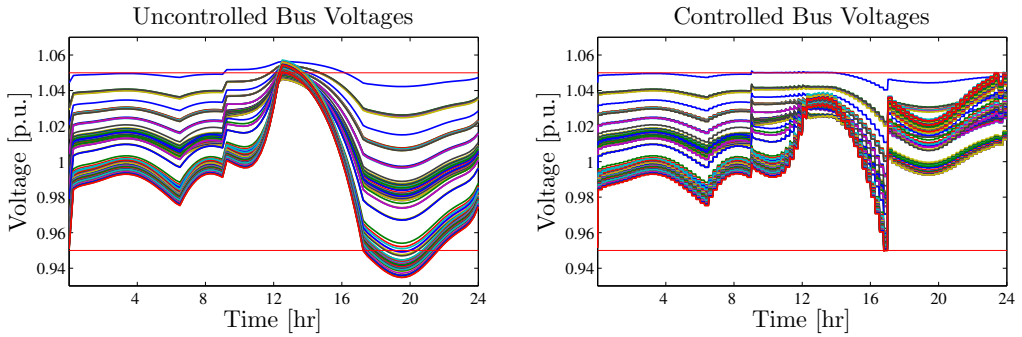


(a) Base Voltage Case

(b) Controlled Voltage Case

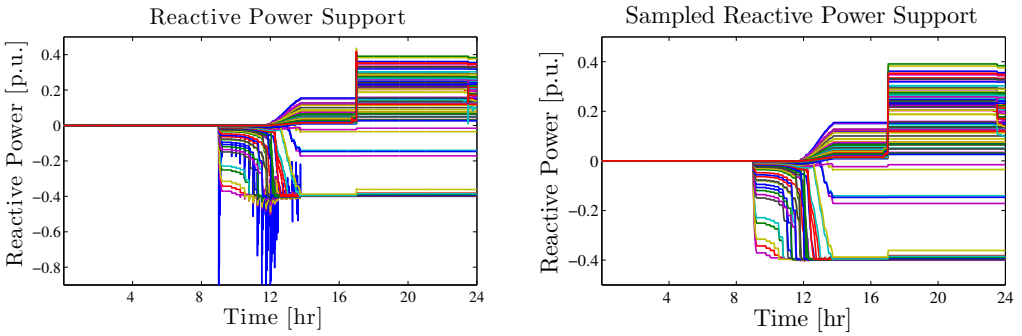


(c) Reactive Power Support

(d) Sampled

Figure 5.15: Case 2 for the 123 Node Network

## Case 3: Afternoon Cloud Cover

The third case is the reversal of the second. Buses 1 through 65 are based on the PV curve in Fig. 5.1c, and the remaining buses are developed from

Fig. 5.1d. The uncontrolled and controlled bus voltages are shown in Figs. 5.16a and 5.16b. Intuitively, the contributions of the nodes in this case will be similar to the results in case 1 since the active power injections prior to the peak at noon are equivalent. Figures 5.16c and 5.16d show that once the active power produced by the PV systems drops, they maintain their current values until they have to suddenly correct for the under-voltage that develops from the increased system loads in the evening.

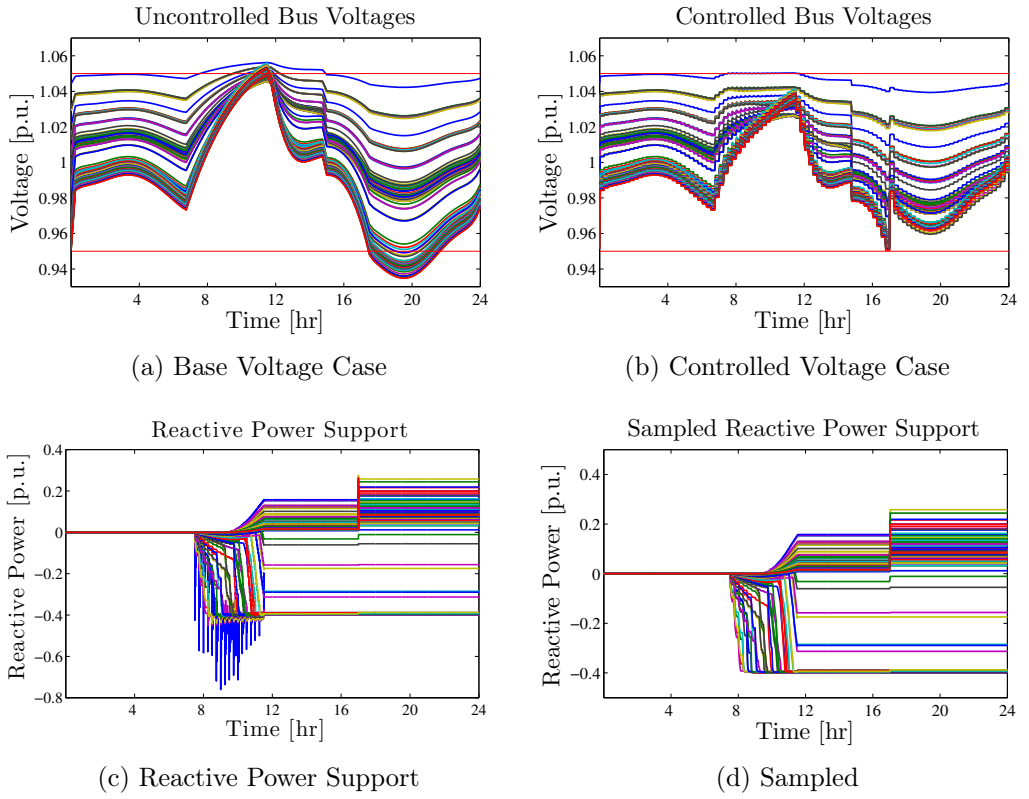


(a) Base Voltage Case

(b) Controlled Voltage Case

(c) Reactive Power Support

(d) Sampled

Figure 5.16: Case 3 for the 123 Node Network

## Case 4: Intermittent Cloud Cover

In the final case, the PV system's active power injections follow the curve in Fig. 5.1b. In the uncontrolled voltage plots, there are three over-voltages primarily on buses 2 through 8 that correspond to the jumps in active power production of the PV systems at 9:00 A.M., noon, and 1:30 P.M. as shown in Fig. 5.17a and 5.17b. The nodes adjust their loads to correct for the first two violations. The third violation at 1:30 P.M. does not require additional

reactive power since it develops after the peak and the current loads are sufficient to prevent another over-voltage. Similarly to the previous cases, the nodes have to have to correct for an under-voltage that happens from 4:00 P.M. to 7:00 P.M. The reactive power support provided by the nodes is shown in Figs. 5.17c and 5.17d.

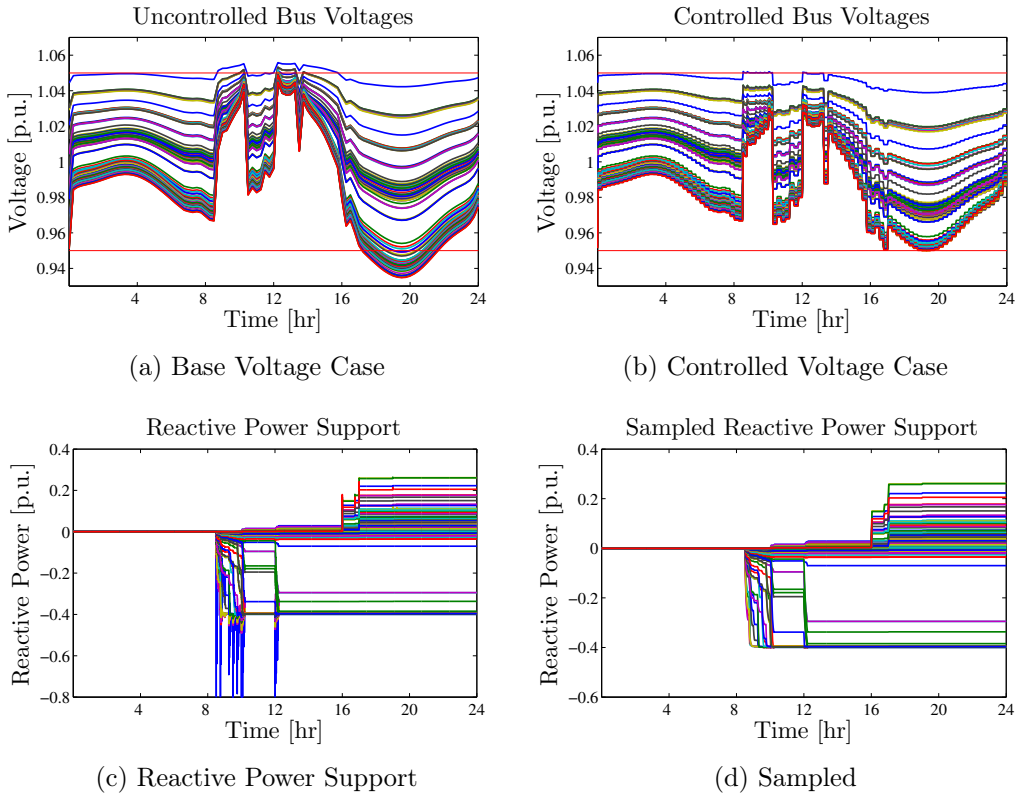


(a) Base Voltage Case

(b) Controlled Voltage Case

(c) Reactive Power Support

(d) Sampled

Figure 5.17: Case 4 for the 123 Node Network

### 5.4.2 Impacts of Sample Periods on Convergence

The reactive power injections that occur between noon and 5:00 P.M. in the 123 bus network are a result of the algorithm correcting for an insufficient number of iterations to properly reach a steady-state solution, which was described in Section 4.3.1. Although the adaptive transition matrix will converge quickly for these corrections, some of the mass will propagate around the system. Increasing the number of iterations that the algorithm runs will decrease the capacity limit violations/corrections previously observed. Figures 5.18a to 5.18d show the system responses when the nominal case for

the 123 bus distribution network is repeated with the iteration sample period changed to 0.002 sec, which is equivalent to 2.5 times the number of iteration steps that were previously allotted. The reactive power injections that were used to prevent lower limit violations are gone. However, the disadvantage of these favorable results is that, given a fixed time step, the distributed algorithm will take significantly longer to converge. Although prior results were less than ideal, they are still a feasible solution and they required 750 fewer steps to reach a solution.

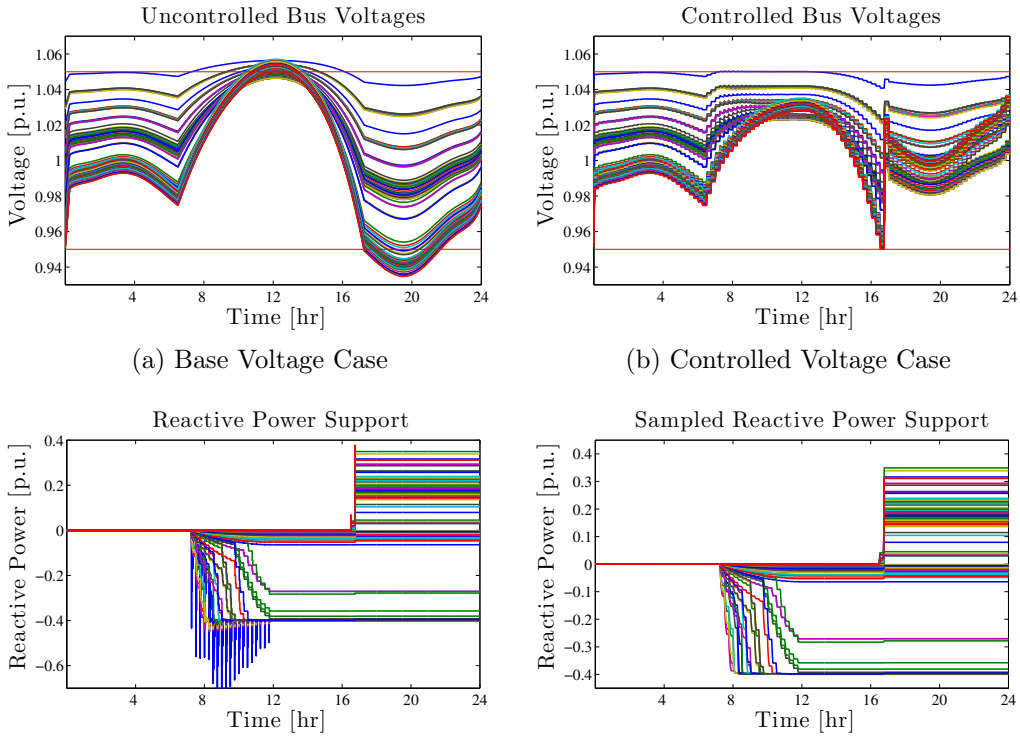


(a) Base Voltage Case

(b) Controlled Voltage Case

(c) Reactive Power Support

(d) Sampled

Figure 5.18: Case 1 for the 123 Node Network with Additional Time to Converge

The results in this case reinforce a common trend for the larger distribution networks: the limit violations and the support needed to correct them are localized to a given region of the network. In each of the four cases, the nodes that behaved as loads typically maintained their values when the nodes that injected reactive power corrected for the under-voltages. This decoupling is evident when the distributed algorithm is given a sufficient number of steps to converge.

### 5.4.3 Constrained 123 Bus Network with Independent Clusters

This case study continues to use the 123 bus distribution network and applies additional constraints on the communication network topology. Rather than every node in the network belonging to a single communicating class, there are five independent communicating classes, or clusters. The clusters are defined in Table 5.4. For example, any node in cluster 1 can respond to an overvoltage on bus 2, but any nodes that belong to the remaining clusters will not react to the voltage violation unless the contingency extends to a bus in that particular cluster. This modified network is equivalent to removing the set of undirected communication links $\{(16, 21), (16, 57), (72, 73), (73, 78)\}$ from the graph representing the network. Each cluster will be strongly connected for all of the nodes that belong to that set.

Table 5.4: Communicating Classes

| Cluster | Nodal Members |
|---|---|
| 1 | 2, 3, 4, 5, 6, 7, 8, 9, 10, 11, 12, 13, 14, 15, 16, 17, 18, 19, 20 |
| 2 | 21, 22, 23, 24, 25, 26, 27, 28, 29, 30, 31, 32, 33, 34, 35, 36, 37, 38, 39, 40, 41, 42, 43, 44, 45, 46, 47, 48, 49, 50, 51, 52, 53, 54, 55, 56 |
| 3 | 57, 58, 59, 60, 61, 62, 63, 64, 65, 66, 67, 68, 69, 70, 71, 72 |
| 4 | 78, 79, 80, 81, 82, 83, 84, 85, 86, 87, 88, 89, 90, 91, 92, 93, 94, 95, 96, 97, 98, 99, 100, 101, 102 |
| 5 | 73, 74, 75, 76, 77, 103, 104, 105, 106, 107, 108, 109, 110, 111, 112, 113, 114, 115, 116, 117, 118, 119, 120, 121, 122, 123 |

Figure 5.11 continues to be the system response without generation from the PV system or reactive power support from the nodes. Due to the similarities in the results to the previous case study, only two weather profiles were used to observe the system response to the new communication network.

## Case 1: Nominal PV Injections

The first case assumes that the PV system experiences nominal sunlight exposure. The system response to the PV injections and loads from PHEVs will remain unchanged. The results of the modified communication network are shown in Figs. 5.19b to 5.19d. All of the nodes in cluster 1 quickly reach their maximum loads to address the over-voltage that results from the active power injections of the PV systems. Although over-voltages are not isolated to cluster 1 in the uncontrolled system response, these buses are the first to experience limit violations and react. The loads provided by these nodes are sufficient to prevent over-voltages in the rest of the system. Similarly, the buses that belong to cluster 5 are the first to experience an under-voltage at 4:45 P.M. and react immediately by supplying reactive power to increase the bus voltages. As the load continues to increase, there is a second jump at 5:00 P.M. These injections increase bus voltages enough that node in clusters 1 to 4 do not experience any under-voltages.

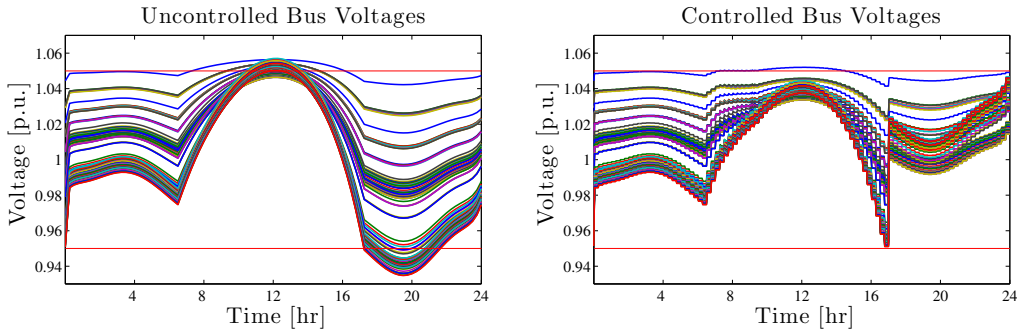


(a) Uncontrolled Voltage Case

(b) Controlled Voltage Case

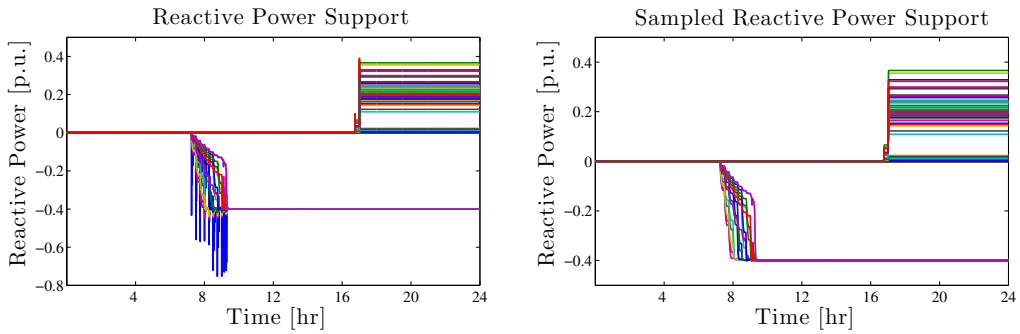


(c) Reactive Power Support

(d) Sampled

Figure 5.19: Case 1 for the Modified 123 Node Network

At the peak PV active power production, there are 86 buses that experience

an over-voltage in Fig. 5.19a. After the control is implemented, the only over-voltage that occurs is on bus 2. The communication gaps between the clusters prevent any nodes from additional clusters from providing support to correct the limit violation on bus 2. However, the combination of using the distributed algorithm(s) with a more traditional approach of adjusting the TCUL transformer could easily correct this minor violation.

In the previous cases, the initial conditions used to ensure that capacity constraints are adhered to caused noticeable injections that were unnecessary across the network. Although the solution was not ideal, it was feasible. The highly constrained case in cluster 1 shows that this strategy is effective and keeps the loads within $\pm 0.001$ p.u. of the $-0.4$ lower bound.

Notice that the system does not require reactive power support from clusters 2, 3, and 4. Comparatively, the previous $\pi_j$'s for these clusters were nonzero. This is easily explained since the entire system was a single, irreducible communicating class, which implies the steady-state values for every node in the system will be nonzero. However, the magnitudes of the steady-state values are inversely proportional to the distance from the violation. Figure 5.18d suggested that the nodes consuming versus those injecting reactive power were decoupled, and Fig. 5.19d confirms this.

### Case 4: Intermittent Cloud Cover

This case shares the same uncontrolled voltage response as the previous case study in Fig. 5.17a. Figures 5.20b to 5.20d are the system responses to the PV profile in Fig. 5.1b and the modified communication network. Clearly, the results for the ideal active power injections in the previous section extend to this example as well. The nodes that consume and inject reactive power are completely decoupled and react accordingly to the changes in active power generation from the PV systems. The system was able to minimize the over-voltages to a single bus, which can be corrected by adjusting the tap on the TCUL transformer.

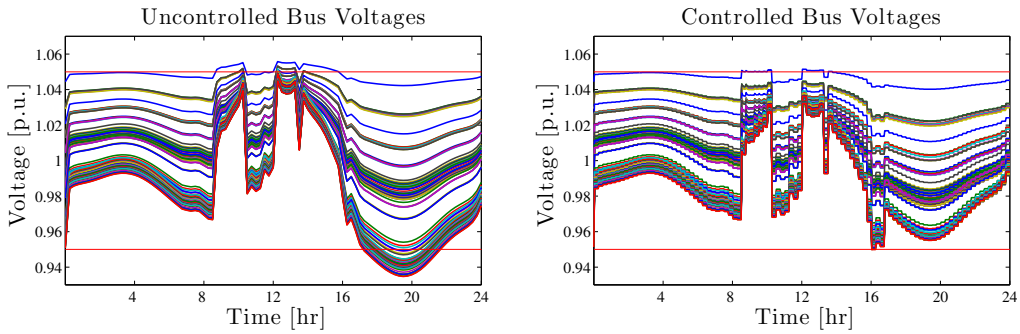


(a) Uncontrolled Voltage Case

(b) Controlled Voltage Case

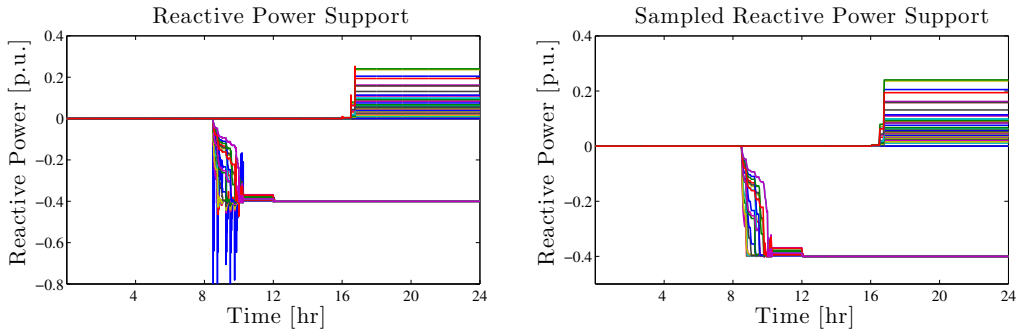


(c) Reactive Power Support

(d) Sampled

Figure 5.20: Case 4 for the Modified 123 Node Network

The case study illustrates several advantages to a system with multiple independent clusters. The reactive power support provided by the nodes is isolated to the clusters that contain the limit violations. This also allows the system to converge faster because there are fewer nodes to communicate with. The second largest eigenvalue dictates the convergence rate of a discrete, linear recursive algorithm. In Section 5.4.1, the second largest eigenvalue for the initial transition matrix is $\lambda = 0.9993$ versus $\lambda = 0.9951$ for this system. The number of iterations for this control strategy is critical to converge within a specified time frame and is proportional to the number of nodes in the cluster.

The disadvantages of the modified communication structure become apparent if the system has aggressive capacity constraints or is operating near node capacities. These case studies illustrate that it may not be possible for a system with independent clusters to recover from a limit violation under these operating conditions. For example, consider an under-voltage situation in a cluster at the end of a sublateral. If the reactive power injection capaci-

ties are insufficient to clear this violation, the resources outside of the cluster will not inject more reactive power if their current measurements are acceptable. Similarly for an over-voltage case, the nodes further down the laterals could potentially consume more reactive power to lower bus voltages. Unfortunately, they will never update their values if every node in their cluster is within operating specifications and the over-voltage will not be resolved.

## 5.5 Chapter Summary

This chapter demonstrates the ability of the distributed voltage control scheme described in Chapter 4 to correct for over-voltages and under-voltages with limited system constraints. Additionally, the three case studies illustrate how potential limit violations can occur due to active power injections in networks with a high penetration of PV systems, particularly when the system is operating near its specified voltage limits. When the communication structure of the system is modified by dropping a few communication links, the nodes are still able to correct for most of the limit violations. This suggests that limit violations are localized to specific regions of the network, and a more robust voltage control strategy may include several communication classes combined with traditional methods.

# Chapter 6

# CONCLUDING REMARKS AND FUTURE WORK

## 6.1 Conclusion

In this thesis, an adaptive distributed algorithm was proposed. This method depends heavily on the convergence of nonnegative matrices and is the natural progression of the constrained fair splitting algorithm presented in Chapter 3. The localized control scheme strategy has limited applications in a large distribution network since it does not account for the voltage profiles of the radial lines. However, it is an extremely effective algorithm for resource allocation for small systems that have small variations in voltage measurements across the system

The greatest advantage of the distributed algorithm for voltage control presented in Chapter 4 is its ability to coordinate resources relative to bus sensitivities. This was illustrated in the case studies performed in Chapter 5. The 123 bus system responses suggested that nodes could be grouped into separate communicating classes, or clusters, and the algorithm would still remain effective. Although the results in a highly constrained environment showed that this limited communication structure was unable to correct for every limit violation, traditional approaches to the voltage regulation problem augmented with this distributed algorithm could prove to be an effective strategy. Furthermore, this would minimize the switching actions of existing equipment and increase the lifetime of components.

## 6.2 Future Work

The work presented in this thesis illustrates the potential of distributed algorithms to aid in the creation of distribution networks with decentralized

control. In Chapter 5 the taps on the TCUL were held constant; future work will incorporate the dynamics of current hardware to develop a more robust control strategy that can realistically be integrated into existing distribution networks.

Although the distributed algorithms were effective in simulation, the convergence times need to be reduced for physical testing to commence. The time constants for TCUL transformers are approximately 30 s, which implies the algorithms are required to correct limit violations in less time to be considered an effective control strategy. The challenge of implementing distributed algorithms into physical systems is to overcome the limitations associated with the baud rates, error corrections, time synchronization issues, etc. The initialization process at each step also needs to be addressed. The method presented in this thesis resembles a proportional controller. In order to improve overall system response time, different controllers must be considered. For example, a PI controller can reference past values for a more accurate estimation to initialize the system with at each step. This will help reduce the number of steps needed to reach a solution.

The effects of the implementation of these devices are relatively unknown. Consider the situation where a communication link between two nodes becomes severed, directional, or intermittent. In addition to physical component failure, faults associated with data computations and transmission could have serious repercussions on system stability and performance. A critical component of future work is to understand the possible failure modes of this methodology.

# Appendix A

# NONNEGATIVE MATRICES

The following definitions are cited from [24].

$\lambda \in \mathbb{C}$ is considered to be an *eigenvalue* of $A \in \mathbb{R}^{n\times n}$ if for $x \in \mathbb{C}$ and

$$Ax = \lambda x \quad x \neq 0. \tag{A.1}$$

Then $x$ is considered the *eigenvector* of $A$ associated with $\lambda$.

The *spectrum* of $A$ is $\sigma(A) := \{\lambda_i : \lambda_i \in \mathbb{C},\, i = 1,\, 2,\, \ldots,\, n\}$ and the *spectral radius* of $A$ is nonnegative real number $\rho(A) = \max\{|\lambda| : \lambda \in \sigma(A)\}$.

## Perron-Frobenius Theorem

Let $A \in \mathbb{R}^{n\times n}$ and suppose that $A$ is irreducible and nonnegative. Then

a. $\rho(A) > 0$

b. $\rho(A)$ is an eigenvalue of $A$

c. There is a positive vector $x$ such that $Ax = \rho(A)\, x$; and

d. $\rho(A)$ is an algebraically simple eigenvalue of $A$.

This version of Perron's theorem is generalized for nonnegative irreducible matrices.

A matrix is considered to be *primitive* if it is irredicible and has only one eiganvalue of maximum modulus, $\rho(A)$.

# Appendix B

# 123 BUS DISTRIBUTION SYSTEM VALUES

Table B.1 contains the bus voltage for the 123 bus distribution network when it reaches its low without PV or PHEV. The capacities for the PV systems and the maximum loads for PHEV are listed.

Table B.1: 123 Bus Distribution Network Values

| Bus | $\|V\|$ | $P_L$ | $Q_L$ | $P_{PV}^{cap}$ | $P_{PHEV}^{cap}$ | $\pi^{max}$ |
|---|---|---|---|---|---|---|
| 1 | 1.0585 | - | - | - | - | - |
| 2 | 1.0444 | 0 | 0 | 0 | 0 | $\pm$ 0.4 |
| 3 | 1.0304 | 0.3799 | 0.1900 | 0.5319 | 0.0760 | $\pm$ 0.4 |
| 4 | 1.0298 | 0 | 0 | 0 | 0 | $\pm$ 0.4 |
| 5 | 1.0296 | 0.3799 | 0.1900 | 0.5319 | 0.0760 | $\pm$ 0.4 |
| 6 | 1.0293 | 0.1900 | 0.0950 | 0.2659 | 0.0380 | $\pm$ 0.4 |
| 7 | 1.0290 | 0.3799 | 0.1900 | 0.5319 | 0.0760 | $\pm$ 0.4 |
| 8 | 1.0303 | 0.1900 | 0.0950 | 0.2659 | 0.0380 | $\pm$ 0.4 |
| 9 | 1.0206 | 0.1900 | 0.0950 | 0.2659 | 0.0380 | $\pm$ 0.4 |
| 10 | 1.0142 | 0 | 0 | 0 | 0 | $\pm$ 0.4 |
| 11 | 1.0141 | 0.1900 | 0.0950 | 0.2659 | 0.0380 | $\pm$ 0.4 |
| 12 | 1.0136 | 0.3799 | 0.1900 | 0.5319 | 0.0760 | $\pm$ 0.4 |
| 13 | 1.0130 | 0 | 0 | 0 | 0 | $\pm$ 0.4 |
| 14 | 1.0129 | 0.1900 | 0.0950 | 0.2659 | 0.0380 | $\pm$ 0.4 |
| 15 | 1.0128 | 0.3799 | 0.1900 | 0.5319 | 0.0760 | $\pm$ 0.4 |

Table B.1: CONTINUED

| Bus | $\|V\|$ | $P_L$ | $Q_L$ | $P_{PV}^{cap}$ | $P_{PHEV}^{cap}$ | $\pi^{max}$ |
|---|---|---|---|---|---|---|
| 16 | 1.0051 | 0 | 0 | 0 | 0 | ± 0.4 |
| 17 | 1.0047 | 0.3799 | 0.1900 | 0.5319 | 0.0760 | ± 0.4 |
| 18 | 1.0045 | 0 | 0 | 0 | 0 | ± 0.4 |
| 19 | 1.0041 | 0.3799 | 0.1900 | 0.5319 | 0.0760 | ± 0.4 |
| 20 | 1.0044 | 0.1900 | 0.0950 | 0.2659 | 0.0380 | ± 0.4 |
| 21 | 0.9963 | 0 | 0 | 0 | 0 | ± 0.4 |
| 22 | 0.9958 | 0.3799 | 0.1900 | 0.5319 | 0.0760 | ± 0.4 |
| 23 | 0.9955 | 0.3799 | 0.1900 | 0.5319 | 0.0760 | ± 0.4 |
| 24 | 0.9953 | 0 | 0 | 0 | 0 | ± 0.4 |
| 25 | 0.9947 | 0.3799 | 0.1900 | 0.5319 | 0.0760 | ± 0.4 |
| 26 | 0.9945 | 0 | 0 | 0 | 0 | ± 0.4 |
| 27 | 0.9939 | 0.3799 | 0.1900 | 0.5319 | 0.0760 | ± 0.4 |
| 28 | 0.9938 | 0 | 0 | 0 | 0 | ± 0.4 |
| 29 | 0.9935 | 0.3799 | 0.1900 | 0.5319 | 0.0760 | ± 0.4 |
| 30 | 0.9932 | 0.3799 | 0.1900 | 0.5319 | 0.0760 | ± 0.4 |
| 31 | 0.9930 | 0.3799 | 0.1900 | 0.5319 | 0.0760 | ± 0.4 |
| 32 | 0.9930 | 0 | 0 | 0 | 0 | ± 0.4 |
| 33 | 0.9934 | 0 | 0 | 0 | 0 | ± 0.4 |
| 34 | 0.9933 | 0 | 0 | 0 | 0 | ± 0.4 |
| 35 | 0.9932 | 0.1900 | 0.0950 | 0.2659 | 0.0380 | ± 0.4 |
| 36 | 0.9931 | 0.1900 | 0.0950 | 0.2659 | 0.0380 | ± 0.4 |
| 37 | 0.9928 | 0.3799 | 0.1900 | 0.5319 | 0.0760 | ± 0.4 |
| 38 | 0.9940 | 0 | 0 | 0 | 0 | ± 0.4 |
| 39 | 0.9918 | 0.3799 | 0.1900 | 0.5319 | 0.0760 | ± 0.4 |

Table B.1: CONTINUED

| Bus | $\|V\|$ | $P_L$ | $Q_L$ | $P_{PV}^{cap}$ | $P_{PHEV}^{cap}$ | $\pi^{max}$ |
|---|---|---|---|---|---|---|
| 40 | 0.9911 | 0 | 0 | 0 | 0 | ± 0.4 |
| 41 | 0.9908 | 0.3799 | 0.1900 | 0.5319 | 0.0760 | ± 0.4 |
| 42 | 0.9909 | 0.1900 | 0.0950 | 0.2659 | 0.0380 | ± 0.4 |
| 43 | 0.9907 | 0.1900 | 0.0950 | 0.2659 | 0.0380 | ± 0.4 |
| 44 | 0.9906 | 0 | 0 | 0 | 0 | ± 0.4 |
| 45 | 0.9905 | 0.1900 | 0.0950 | 0.2659 | 0.0380 | ± 0.4 |
| 46 | 0.9896 | 0.1900 | 0.0950 | 0.2659 | 0.0380 | ± 0.4 |
| 47 | 0.9891 | 0.3799 | 0.1900 | 0.5319 | 0.0760 | ± 0.4 |
| 48 | 0.9889 | 0 | 0 | 0 | 0 | ± 0.4 |
| 49 | 0.9887 | 0.1900 | 0.0950 | 0.2659 | 0.0380 | ± 0.4 |
| 50 | 0.9885 | 0.1900 | 0.0950 | 0.2659 | 0.0380 | ± 0.4 |
| 51 | 0.9881 | 0.3419 | 0.2375 | 0.4787 | 0.0684 | ± 0.4 |
| 52 | 0.9880 | 0.6649 | 0.4749 | 0.9308 | 0.1330 | ± 0.4 |
| 53 | 0.9878 | 0.3324 | 0.2375 | 0.4654 | 0.0665 | ± 0.4 |
| 54 | 0.9876 | 0.3799 | 0.1900 | 0.5319 | 0.0760 | ± 0.4 |
| 55 | 0.9875 | 0.1900 | 0.0950 | 0.2659 | 0.0380 | ± 0.4 |
| 56 | 0.9875 | 0 | 0 | 0 | 0 | ± 0.4 |
| 57 | 0.9978 | 0 | 0 | 0 | 0 | ± 0.4 |
| 58 | 0.9905 | 0.3799 | 0.1900 | 0.5319 | 0.0760 | ± 0.4 |
| 59 | 0.9871 | 0.3799 | 0.1900 | 0.5319 | 0.0760 | ± 0.4 |
| 60 | 0.9850 | 0 | 0 | 0 | 0 | ± 0.4 |
| 61 | 0.9848 | 0.1900 | 0.0950 | 0.2659 | 0.0380 | ± 0.4 |
| 62 | 0.9847 | 0.1900 | 0.0950 | 0.2659 | 0.0380 | ± 0.4 |
| 63 | 0.9793 | 0 | 0 | 0 | 0 | ± 0.4 |

Table B.1: CONTINUED

| Bus | $\|V\|$ | $P_L$ | $Q_L$ | $P_{PV}^{cap}$ | $P_{PHEV}^{cap}$ | $\pi^{max}$ |
|---|---|---|---|---|---|---|
| 64 | 0.9790 | 0.1900 | 0.0950 | 0.2659 | 0.0380 | ± 0.4 |
| 65 | 0.9789 | 0.1900 | 0.0950 | 0.2659 | 0.0380 | ± 0.4 |
| 66 | 0.9676 | 0.1900 | 0.0950 | 0.2659 | 0.0380 | ± 0.4 |
| 67 | 0.9660 | 0.3799 | 0.1900 | 0.5319 | 0.0760 | ± 0.4 |
| 68 | 0.9650 | 0.3799 | 0.1900 | 0.5319 | 0.0760 | ± 0.4 |
| 69 | 0.9634 | 0.7124 | 0.3324 | 0.9973 | 0.1425 | ± 0.4 |
| 70 | 0.9622 | 0.3324 | 0.2375 | 0.4654 | 0.0665 | ± 0.4 |
| 71 | 0.9616 | 0.7124 | 0.3324 | 0.9973 | 0.1425 | ± 0.4 |
| 72 | 0.9635 | 0 | 0 | 0 | 0 | ± 0.4 |
| 73 | 0.9595 | 0 | 0 | 0 | 0 | ± 0.4 |
| 74 | 0.9588 | 0.1900 | 0.0950 | 0.2659 | 0.0380 | ± 0.4 |
| 75 | 0.9581 | 0.3799 | 0.1900 | 0.5319 | 0.0760 | ± 0.4 |
| 76 | 0.9576 | 0.1900 | 0.0950 | 0.2659 | 0.0380 | ± 0.4 |
| 77 | 0.9573 | 0.3799 | 0.1900 | 0.5319 | 0.0760 | ± 0.4 |
| 78 | 0.9583 | 0 | 0 | 0 | 0 | ± 0.4 |
| 79 | 0.9575 | 0.3799 | 0.1900 | 0.5319 | 0.0760 | ± 0.4 |
| 80 | 0.9567 | 0.3799 | 0.1900 | 0.5319 | 0.0760 | ± 0.4 |
| 81 | 0.9563 | 0.3799 | 0.1900 | 0.5319 | 0.0760 | ± 0.4 |
| 82 | 0.9578 | 0.6649 | 0.4749 | 0.9308 | 0.1330 | ± 0.4 |
| 83 | 0.9578 | 0.3799 | 0.1900 | 0.5319 | 0.0760 | ± 0.4 |
| 84 | 0.9578 | 0 | 0 | 0 | 0 | ± 0.4 |
| 85 | 0.9577 | 0.3799 | 0.1900 | 0.5319 | 0.0760 | ± 0.4 |
| 86 | 0.9582 | 0.3799 | 0.1900 | 0.5319 | 0.0760 | ± 0.4 |
| 87 | 0.9589 | 0 | 0 | 0 | 0 | ± 0.4 |

Table B.1: CONTINUED

| Bus | $\|V\|$ | $P_L$ | $Q_L$ | $P_{PV}^{cap}$ | $P_{PHEV}^{cap}$ | $\pi^{max}$ |
|---|---|---|---|---|---|---|
| 88 | 0.9595 | 0.3799 | 0.1900 | 0.5319 | 0.0760 | ± 0.4 |
| 89 | 0.9602 | 0.1900 | 0.0950 | 0.2659 | 0.0380 | ± 0.4 |
| 90 | 0.9578 | 0.1900 | 0.0950 | 0.2659 | 0.0380 | ± 0.4 |
| 91 | 0.9573 | 0.3799 | 0.1900 | 0.5319 | 0.0760 | ± 0.4 |
| 92 | 0.9570 | 0.1900 | 0.0950 | 0.2659 | 0.0380 | ± 0.4 |
| 93 | 0.9566 | 0.3799 | 0.1900 | 0.5319 | 0.0760 | ± 0.4 |
| 94 | 0.9564 | 0 | 0 | 0 | 0 | ± 0.4 |
| 95 | 0.9562 | 0 | 0 | 0 | 0 | ± 0.4 |
| 96 | 0.9560 | 0 | 0 | 0 | 0 | ± 0.4 |
| 97 | 0.9558 | 0.1900 | 0.0950 | 0.2659 | 0.0380 | ± 0.4 |
| 98 | 0.9566 | 0.3799 | 0.1900 | 0.5319 | 0.0760 | ± 0.4 |
| 99 | 0.9564 | 0.3799 | 0.1900 | 0.5319 | 0.0760 | ± 0.4 |
| 100 | 0.9562 | 0.3799 | 0.1900 | 0.5319 | 0.0760 | ± 0.4 |
| 101 | 0.9557 | 0.3799 | 0.1900 | 0.5319 | 0.0760 | ± 0.4 |
| 102 | 0.9557 | 0.1900 | 0.0950 | 0.2659 | 0.0380 | ± 0.4 |
| 103 | 0.9580 | 0 | 0 | 0 | 0 | ± 0.4 |
| 104 | 0.9576 | 0.3799 | 0.1900 | 0.5319 | 0.0760 | ± 0.4 |
| 105 | 0.9570 | 0.3799 | 0.1900 | 0.5319 | 0.0760 | ± 0.4 |
| 106 | 0.9569 | 0.3799 | 0.1900 | 0.5319 | 0.0760 | ± 0.4 |
| 107 | 0.9569 | 0 | 0 | 0 | 0 | ± 0.4 |
| 108 | 0.9570 | 0 | 0 | 0 | 0 | ± 0.4 |
| 109 | 0.9559 | 0 | 0 | 0 | 0 | ± 0.4 |
| 110 | 0.9553 | 0.1900 | 0.0950 | 0.2659 | 0.0380 | ± 0.4 |
| 111 | 0.9546 | 0.3799 | 0.1900 | 0.5319 | 0.0760 | ± 0.4 |

Table B.1: CONTINUED

| Bus | $\|V\|$ | $P_L$ | $Q_L$ | $P_{PV}^{cap}$ | $P_{PHEV}^{cap}$ | $\pi^{max}$ |
|---|---|---|---|---|---|---|
| 112 | 0.9539 | 0.3799 | 0.1900 | 0.5319 | 0.0760 | ± 0.4 |
| 113 | 0.9551 | 0 | 0 | 0 | 0 | ± 0.4 |
| 114 | 0.9546 | 0.3799 | 0.1900 | 0.5319 | 0.0760 | ± 0.4 |
| 115 | 0.9540 | 0.3799 | 0.1900 | 0.5319 | 0.0760 | ± 0.4 |
| 116 | 0.9545 | 0 | 0 | 0 | 0 | ± 0.4 |
| 117 | 0.9545 | 0 | 0 | 0 | 0 | ± 0.4 |
| 118 | 0.9528 | 0.3799 | 0.1900 | 0.5319 | 0.0760 | ± 0.4 |
| 119 | 0.9520 | 0 | 0 | 0 | 0 | ± 0.4 |
| 120 | 0.9517 | 0.1900 | 0.0950 | 0.2659 | 0.0380 | ± 0.4 |
| 121 | 0.9518 | 0.1900 | 0.0950 | 0.2659 | 0.0380 | ± 0.4 |
| 122 | 0.9509 | 0.3799 | 0.1900 | 0.5319 | 0.0760 | ± 0.4 |
| 123 | 0.9507 | 0.1900 | 0.0950 | 0.2659 | 0.0380 | ± 0.4 |

# REFERENCES


[1] G. Joos, B. T. Ooi, D. McGillis, F. D. Galiana, and R. Marceau, "The potential of distributed generation to provide ancillary services," in *Power Engineering Society Summer Meeting, 2000. IEEE*, vol. 3, 2000, pp. 1762–1767.

[2] M. E. Baran and I. M. El-Markabi, "A multiagent-based dispatching scheme for distributed generators for voltage support on distribution feeders," *IEEE Transactions on Power Systems*, vol. 22, no. 1, pp. 52–59, February 2007.

[3] C. Guille, "A conceptual framework for the vehicle-to-grid (V2G) implementation," M.S. thesis, University of Illinois at Urbana-Champaign, Urbana, IL, February 2009.

[4] A. D. Dominguez-Garcia and C. N. Hadjicostis, "Coordination and control of distributed energy resources for provision of ancillary services," in *IEEE International Conference on Smart Grid Communications*, Gaithersburg, MD, October 2010, pp. 537–542.

[5] H. Li, F. Li, Y. Xu, D. Rizy, and J. Kueck, "Adaptive voltage control with distributed energy resources: Algorithm, theoretical analysis, simulation, and field test verification," *IEEE Transactions on Power System*, vol. 25, no. 3, pp. 1638–1647, August 2010.

[6] "Costs and emissions associated with plug-in hybrid electric vehicle charging in the Xcel Energy Colorado service territory," National Renewable Energy Laboratory, Tech. Rep. TP-640-41410, January 2007.

[7] "Field testing plug-in hybrid electric vehicles with charge control technology in the Xcel Energy territory," National Renewable Energy Laboratory, Tech. Rep. TP-550-46345, August 2009.

[8] S. Shao, T. Zhang, M. Pipattanasomporn, and S. Rahman, "Impact of TOU rates on distribution load shapes in a smart grid with PHEV penetration," in *IEEE PES Transmission and Distribution Conference and Exposition, 2010*, April 2010, pp. 1–6.

[9] T. V. Cutsem and C. Vournas, *Voltage Stability of Electric Power Systems*. Norwell, MA: Kluwer Academic Publishers, 1998.

[10] J. D. Glover, M. S. Sarma, and T. J. Overbye, *Power System Analysis and Design*, 4th ed. Stamford, CT: Cengage Learning, 2008.

[11] "2008 wind technologies market report," National Renewable Energy Laboratory, Tech. Rep. TP-6A2-46026, July 2009.

[12] "2008 solar technologies market report: January 2010," National Renewable Energy Laboratory, Tech. Rep. TP-6A2-46025, January 2010.

[13] Y. Ueda, K. Kurokawa, T. Tanabe, K. Kitamura, and H. Sugihara, "Analysis results of output power loss due to the grid voltage rise in grid-connected photovoltaic power generation systems," *IEEE Transactions on Industrial Electronics*, vol. 55, no. 7, pp. 2744–2751, July 2008.

[14] W. H. Kersting, *Distribution System Modeling and Analysis*. New York, NY: CRC Press, 2001.

[15] "IEEE application guide for IEEE Std 1547, IEEE standard for interconnecting distributed resources with electric power systems," *IEEE Std 1547.2-2008*, pp. 1–207, April 2009.

[16] K. Turitsyn, P. Sulc, S. Backhaus, and M. Chertkov, "Distributed control of reactive power flow in a radial distribution circuit with high photovoltaic penetration," in *IEEE Power and Energy Society General Meeting, 2010*, Minneapolis, MN, July 2010, pp. 1–6.

[17] P. Carvalho, P. Correia, and L. Ferreira, "Distributed reactive power generation control for voltage rise mitigation in distribution networks," *IEEE Transactions on Power System*, vol. 23, no. 2, pp. 766–772, May 2008.

[18] T. Senjyu, Y. Miyazato, A. Yona, N. Urasaki, and T. Funabashi, "Optimal distribution voltage control and coordination with distributed generation," *IEEE Transactions on Power Delivery*, vol. 23, no. 2, pp. 1236–1242, April 2008.

[19] D. Schooley, Written communication from an engineer at ComEd, March 2011.

[20] K. Rogers, R. Klump, H. Khurana, A. Aquino-Lugo, and T. Overbye, "An authenticated control framework for distributed voltage support on the smart grid," *IEEE Transactions on Smart Grid*, vol. 1, no. 1, pp. 40–47, June 2010.

[21] A. Aquino-Lugo, "Distributed and decentralized control of the power grid," Ph.D. dissertation, University of Illinois at Urbana-Champaign, Urbana, IL, December 2010.

[22] R. Olfati-Saber, J. A. Fax, and R. M. Murray, "Consensus and cooperation in networked multi-agent systems," *Proceedings of the IEEE*, vol. 95, no. 1, pp. 215 –233, January 2007.

[23] P. W. Sauer and M. A. Pai, *Power System Dynamics and Stability*. Champaign, IL: Stipes Publishing, 2006.

[24] R. A. Horn and C. R. Johnson, *Matrix Analysis*, 23rd ed. New York, NY: Cambridge University Press, 2010.

[25] J. A. Bondy and U. S. R. Murty, *Graph Theory*, 2nd ed. New York, NY: Springer, 2008.

[26] J. R. Norris, *Markov Chains*, 15th ed. New York, NY: Cambridge University Press, 2009.

[27] E. Seneta, *Non-negative Matrices and Markov Chains*. New York, NY: Springer, 2006.

[28] G. F. Franklin, J. D. Powell, and M. Workman, *Digital Control of Dynamic Systems*, 3rd ed. Half Moon Bay, CA: Ellis-Kagle Press, 2006.

[29] A. Keane, L. Ochoa, E. Vittal, C. Dent, and G. Harrison, "Enhanced utilization of voltage control resources with distributed generation," *IEEE Transactions on Power System*, vol. 26, no. 1, pp. 252–260, February 2011.

[30] S. V. Dhople, J. L. Ehlmann, C. J. Murray, S. T. Cady, and P. Chapman, "Engineering systems in the gable home: A passive, net-zero, solar-powered house for the U. S. Department of Energy's 2009 Solar Decathlon," in *Power and Energy Conference at Illinois (PECI), 2010*, February 2010, pp. 58–62.

[31] University of Nevada, "Measurement and instrumentation data center," March 2011. [Online]. Available: http://www.nrel.gov/midc/unlv/

[32] PJM, "Historical metered load data," March 2011. [Online]. Available: http://www.pjm.com/markets-and-operations/compliance/nerc-standards/historical-load-data.aspx

[33] IEEE Power & Energy Society, "Distribution test feeders," September 2010. [Online]. Available: http://www.ewh.ieee.org/soc/pes/dsacom/testfeeders/index.html